Review

A review of applications of CT imaging on fiber reinforced composites

Yantao Gao[1] ⓘ**, Wenfeng Hu[1], Sanfa Xin[1] and Lijuan Sun[2]**

Abstract

With the development of X-ray computed tomography over the last few decades, it is gradually considered to be a powerful tool in the field of materials research. This paper presents a comprehensive review of applications of CT imaging on fiber reinforced composites, from polymer composites to ceramic matrix composites. The principle of X-ray CT and experimental tomography setups was described firstly. Then, in situ experimental devices developed in recent years were illustrated. Furthermore, the applications of X-ray CT imaging on manufacturing process, modeling, mechanical damage, physical, and chemical behaviors were reviewed in detail. Besides, advantages and limitations of X-ray CT imaging were pointed out and the future development was prospected.

Keywords

X-ray computed tomography, permeability, microstructure, modeling, failure, mechanical properties

Introduction

Due to multiphase materials, fiber reinforced composites, such as polymer-, metal-, and ceramic matrix composites, are anisotropic and heterogeneous.[1-3] Their deformation behaviors are direction-dependent as the properties of individual constituents are different.[4] In addition, the accumulation of flaws shows complex 3D patterns in the interior of fiber reinforced composites.[5-6] Therefore, microstructure characterization in the composites during manufacturing and under in-service conditions is difficult. Recently, X-ray computed tomography (XCT) has become a powerful tool because of high spatial resolution and the ability to precisely capture the internal 3D multi-scale structures non-destructively.[7-9] XCT has been widely used for qualitative and quantitative assessments in the fields of fiber reinforced composites.[10-25] Compared to other destructive and 2D visualization techniques, such as scanning electron microscopy, optical microscopy, etc., XCT can provide information on the internal microstructure in both 2D and 3D formats.[26] Moreover, other non-destructive techniques, such as ultrasonic C-scan and Acoustic Emission, could detect the defects in the interior, but they cannot capture the high-resolution damage mechanisms which can be achieved using XCT.[27-28] Therefore, the applications of CT imaging on fiber reinforced composites are worth paying attention to.

In liquid molding technologies, such as resin transfer molding (RTM) and vacuum resin infusion, resin is infiltrated into the dry fiber preform by means of a pressure gradient between the inlet and outlet gates.[29] Voids and air entrapments which significantly reduce mechanical properties of the end products are easily formed during infiltration.[30-32] Monitoring accurately void generation and transport and understanding the resin flow mechanisms are crucial to optimize the manufacturing process. The curing conditions also influence the actual volume fraction, shape, and spatial distribution of voids.[33] Furthermore, Chemical Vapor Infiltration (CVI) is widely used in the manufacturing of ceramic matrix composites.[34] In the process, a heated fibrous preform is infiltrated by the chemical cracking of a vapor precursor of the matrix material inside the pore space of the preform. The quality of materials prepared by CVI relies on processing conditions (such as gas precursor concentration, temperature, and pressure), as well as the

[1]School of Textiles and Fashion, Shanghai University of Engineering Science, Shanghai, China
[2]The State Key Laboratory of Nonlinear Mechanics, Institute of mechanics, Chinese academy of sciences, Beijing, China

Corresponding authors:
Yantao Gao, School of Textiles and Fashion, Shanghai University of Engineering Science, No. 333, Longteng Road, Songjiang District, Shanghai 201620, China.
Email: gaoyantao@sues.edu.cn

Lijuan Sun, The State Key Laboratory of Nonlinear Mechanics, Institute of mechanics, Chinese academy of sciences, No. 15 Beisihuanxi Road, Beijing 100190, China.
Email: sunlj@lnm.imech.ac.cn

intrinsic properties of the preform.[35] The transport properties of the preform at various stages of infiltration are of great interest to optimize the final density and homogeneity of the composites. X-ray computed tomography had been successfully used to solve the problems, such as compact characterization,[36-40] permeability characterization,[41-44] void generation, and transform in manufacturing process.[45-48]

As we all know, the quality of FE analyses or DVC mostly depends on the quality of the initial model and its geometry.[49-54] For 2D or 3D textile structural composites, the architectures of the preform are more complicated as the tows crimp and interlace. Although the geometry could be obtained with textile geometrical simulators such as TexGen[55] or WiseTex,[56] they are idealized geometry without taking into account the geometrical imperfections or specificities of the materials. However, the high-resolution of μ-CT enable the visualization of each fiber tow and intra/inter-tow voids that can be directionally introduced to finite element models,[57-58] which will provide a more real geometry of 3D composite reinforcements. Besides, XCT is also suitable regarding 3D textile reinforcements for whose internal geometries are numerous and complex, while it is limited for textile geometrical simulators.[59-60]

Mechanical damage characterization of fiber reinforced composites is critical in understanding their failure mechanisms.[61] As a non-destructive method, XCT has gained great interest as an ideal tool for material mechanics studies from quasi-static mechanics to dynamic mechanics.[62-92] With the capability providing 3D images in the micrometer and submicrometer resolution range, it is being increasingly applied to investigate the initiation and propagation in three-dimensional (3D) bodies non-destructively.[93-94] In recent year, a large number of researchers have focused on failure research of fiber reinforced composites based on lab and synchrotron X-ray sources by in situ or ex situ experiments.[95-101] Especially, the high brightness associated with synchrotron radiation μ-CT (SR μ-CT) enables the rapid acquisition of successive high spatial resolution 3D images to track crack propagation or damage accumulation under monotonic, or cyclic, loads using time-lapse 3D imaging.[102]

Besides, the properties of materials could be degraded or damaged under service conditions, such as moisture,[103] low or high temperature,[104-106] oxygen,[107-108] irradiation[109] and so on.[110] XCT has been utilized to analyze the three-dimensional (3D) morphology of the microstructure of fiber reinforced composites.[108,110] Also, some in situ experiments have been carried out to investigate the behaviors of the materials under the special environments.[111]

Consequently, in this study, we systemically reviewed the applications of XCT on the unique characteristics in fiber reinforced composites field from manufacturing process to performance. Firstly, we introduced the basic principles of XCT before looking at the use of in situ

environments for time-lapse imaging. Then, we outlined in situ experiments developed in recent years. After that, we illustrated the applications of XCT on fiber reinforced composites in detail by practical examples. Finally, we described the limitation of XCT and considered the future opportunities in studying manufacturing process, mechanical damage, and degradation mechanisms.

CT imaging and in situ experiments

The basic principle of CT imaging

Since its first applications in the medical field in the early 1970s, XCT was developed rapidly and soon applied across a wide range of fields, such as materials science, archeology, geology, and biomedical science. In absorption mode X-ray CT, X-rays are attenuated after they interact with an object and the level of attenuation is related to the atomic number of the material.[112] In the range of X-ray energies used for materials, the attenuation coefficient for a specific point (x, y, z) within the materials takes the form[113]

$$\mu(x,y,z) = K\rho \frac{Z^4}{E^3}$$

where K is a constant, ρ is the material density, Z is the material atomic number, and E is the energy of the incident photons.

In phase contrast mode X-ray CT, the refractive index, n, describes the interaction of X-rays with matter[103]

$$n = 1 - \delta + i\beta$$

where the imaginary part (β) describes the attenuation (absorption) and the real part (δ) the phase shift. For XCT, the composite, for example, carbon fiber with low atomic number exhibits low X-ray attenuation, it leads to poor contrast between fibers and matrix and limits the detectability of narrow matrix cracks, even at high spatial resolution. Imaging modes that exploit the phase shift can deliver increased feature detectability relative to simple absorption contrast.

Although various experimental set ups can be used to perform X-ray tomography, the basic principle is the same. Figure 1 shows a schematic illustration of the basic principle of X-ray attenuation tomography: An X-ray beam coming from a laboratory or synchrotron source impinges on a sample mounted on a rotator; For a given angular position of the sample, a radiograph of the sample is recorded and a series of N radiographs corresponding to N angular positions of the sample in the beam is recorded on a detector which is generally a CCD in modern tomography. Those radios are used by a reconstruction software to produce a 3D map of the linear X-ray attenuation coefficient μ within the studied sample. This distribution forms a 3D image in which elementary unit is called a voxel and which can be viewed with appropriate imaging software.

Here, it is only a simply description of XCT. For a more detailed description, one can refer to some classical books and research papers for a comprehensive understanding.[114-116]

In situ experiments

Usually, XCT is classified as in situ and ex situ imaging according to test conditions. In situ imaging is directly performed under load/heat/oxide etc. using an environmental rig mounted on the X-ray CT scanner, while for an ex situ experiment, the sample is removed from the environmental/loading chamber and then placed inside the XCT for further analysis. Both in situ and ex situ imaging can be undertaken repeatedly on a single sample in a time-lapse manner. The results obtained from such experiments are a series of 3D images of the internal microstructure of the material as a function of time. Researchers can investigate the nucleation and propagation of cracks, or defects, or fiber architectural features by tracking the evolution of structure through its manufacturing process or service life.[61,117] Comparing with ex situ imaging, in situ imaging still has significant advantages as removing a sample from its environment may change the state

of the composite. For example, certain features such as transverse cracks may close up after unloading the specimen as described in Figure 2. However, the crack closure effect can be quantified using in situ XCT. For the fiber reinforced composites, manufacturing defects and the propagation of cracks are random and differ significantly from specimen to specimen. Therefore, it is much preferable to work in situ with the sample constantly installed on XCT. The flow chart of in situ experiments is described as in Figure 3.

Nowadays, a large number of rigs have been developed for in situ X-ray CT measurements allowing one to perform in situ tension,[62] compression,[71] bending[118] and even short-term fatigue at ambient temperatures,[119] low temperatures,[106] and elevated temperatures[63] within both laboratory X-ray CT systems or upon synchrotron beamlines. Figure 4 shows some typical ambient in situ devices developed for time-lapse experiments at synchrotron beamlines. Figures 4(a) and (b) separately described a tension/compression rig mounted on the ID19 at the ESRF and a cyclic loading device for fatigue measurement. The detail description of the rigs can be referred in reference.[111] Figures 4(c) and (d) are a monotonic tensile rig used and a typical ambient in situ fatigue test machine developed by Shimadzu
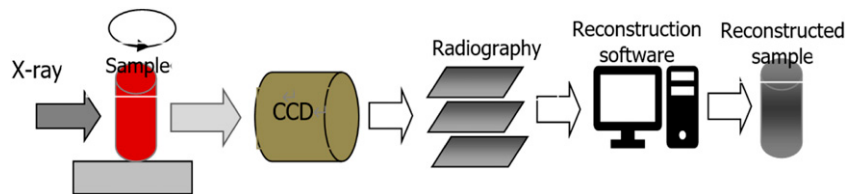

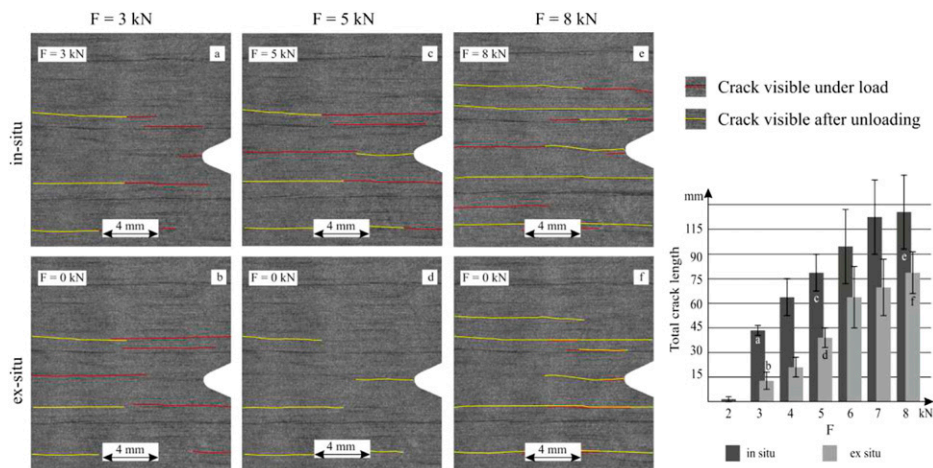**Figure 1.** Schematic illustration of the principle of X-ray computed tomography.

Figure 2. Crack visible based on in situ CT and ex situ CT images of damaged. CF/EP-NCF specimens.[117]

Corporation.[120] There are also some commercialized rigs utilized by lab and synchrotron XCT, as described as in Figure 5. It can be seen that a variety of designs can enable room temperature loading in situ. The great majority of rigs have been designed to be essentially transparent to X-rays by using low X-ray absorption window. The rotation of sample is performed by the rotation of the entire stage or loading axis (in Figure 4(c)). The in situ devices are widely used to analyze the deformation behaviors of materials in tension, compression, or cyclic loading experiments.

Some in situ devices have also been developed to allow mechanical testing at moderate and extreme high temperatures (See Figure 6), and sub-zero temperatures (see Figure 7). Usually, these are extensions of the ambient in situ loading rigs for certain cases. Figure 6(a) shows a compact in situ ultrahigh temperature tensile test rig for XCT at Beamline 8.3.2 of Advanced Light Source. A thin aluminum window has been utilized to allow the x-rays to pass through the chamber. Samples can be loaded in tension or compression with forces up to 2.2 kN. The instrument has been used to characterize the evolution of 3D damage mechanisms in ceramic composite materials under tensile loading at 1750°C. Figure 6(b) is a smart in situ rig in ESRF

for high temperature tensile or compression tests. The heating of the sample is performed via an induction copper coil surrounding the sample gage length. The temperature can reach 1500°C for steel. Figure 6(c) gives a bespoke P2R mechanical test rig mounted on the I12 beamline at Diamond Light Source. It allows simultaneous tension, compression, and/or torsion during tomography, with the measurement precision of 100 nm motion and 0.1 N load. Figure 6(d) shows a dedicated device developed for investigating the mechanical behaviors of the structural materials in molten salt reactor, such as graphite, SiC$_f$/SiC composites. The temperature can reach above 700°C and it allow to work with pressure up to 3 atm. The maximum loading is up to 2000N.

Additionally, an in situ tensile/compression rig with a temperature-controlled mini-oedometer has been used on Beamline I12 at Diamond Light Source. The temperature is controllable. The experiment conducted to study cracks in Frozen Soil had been carried out under 0°C. However, it should be mentioned that in situ devices tend to be quite bulky, therefore limiting how close the X-ray source can get to the specimen, which in turn limits CT resolution in flexible XCT setups.

Applications of CT imaging on fiber reinforced composites

XCT imaging has wide applications on fiber reinforced composites as it can delineate the architecture of the constituent phases, and provide a better understanding of defects introduced during manufacture or damage accumulated in-service. Figure 8 illustrates the main applications consisting of modeling, assessment of manufacturing process, characterization under environmental conditions, and mechanical behaviors under loading. Sometimes, it is overlapping as the sample could face multiple conditions, for example, a sample could be loaded at high temperature.
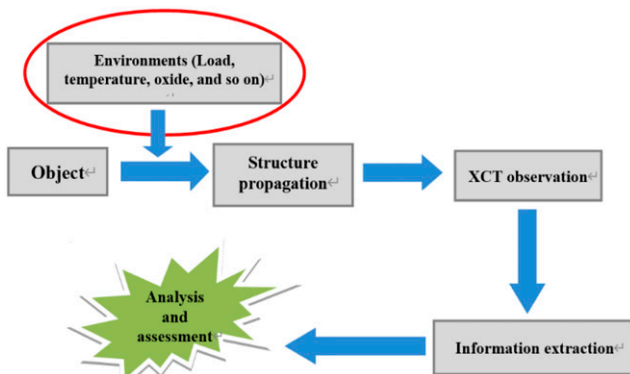

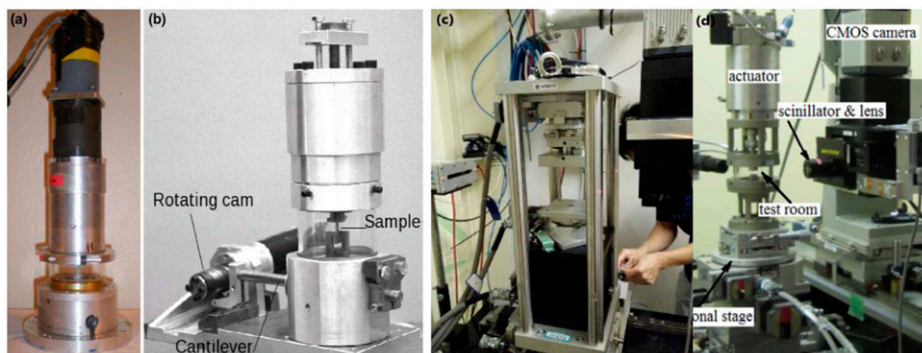**Figure 3.** The flow chart of in situ experiments.

Figure 4. Monotonic tension/compression rig and cyclic loading rig at ambient temperatures. (a) A typical ambient monotonic tension/compression rig at ESRF[111]; (b) Cyclic loading rig at ESRF[111]; (c) Ambient tensile rig; (d) Ambient cyclic loading rig developed by Shimadzu Corporation.[120]
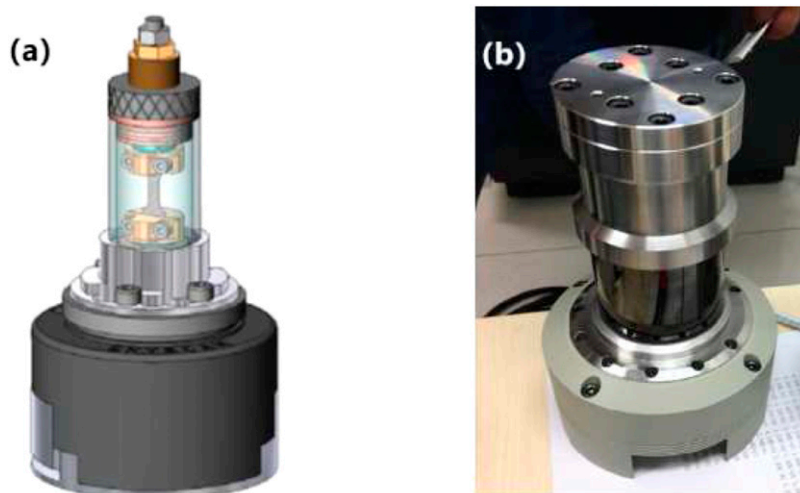
Figure 5. Commercialized rigs utilized by lab and synchrotron X-ray computed tomography. (a) Bruker micro-CT; (b) Deben micro-CT.
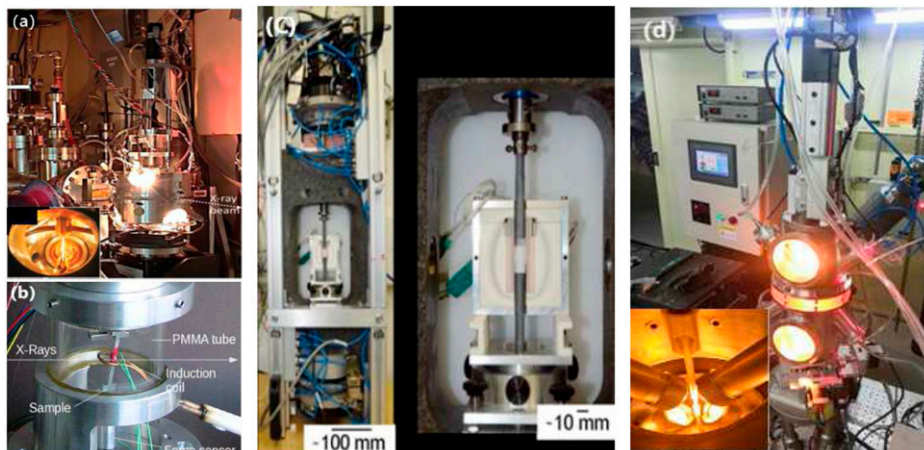

Figure 6. Typical high temperature in situ rigs. (a) at ALS[62]; (b) at ESRF[111]; (c) at DIAMOND Source[121]; (d) at SSRF.
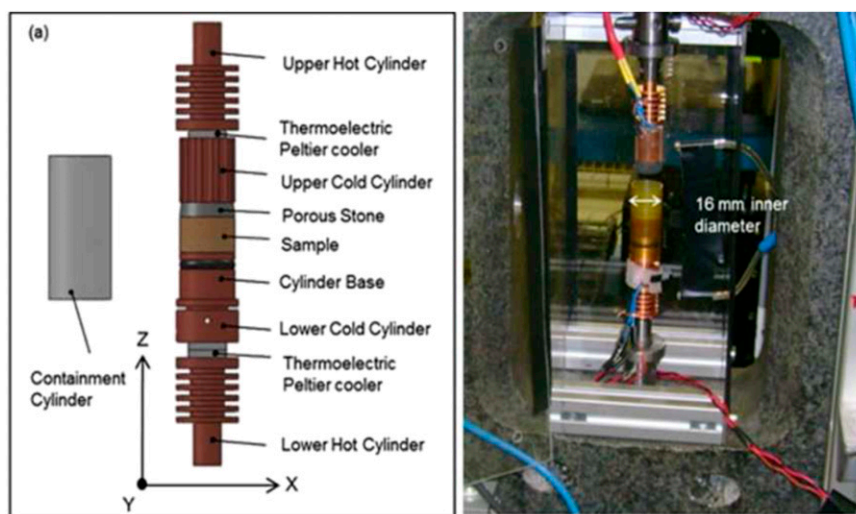

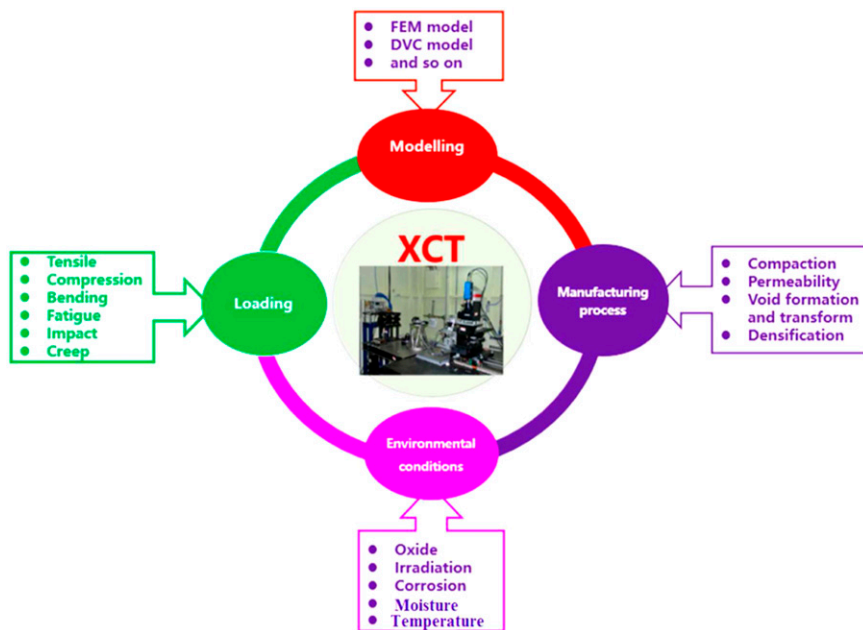**Figure 7.** In situ tensile/compression rig at Diamond Light Source.[106]

Figure 8. Schematic representation of applications of X-ray computed tomography on fiber reinforced composites.

Modeling and microstructure characterization

Modeling. The permeation of the matrix during RTM processes and the mechanical properties of the composites can be effectively predicted by FE analyses. Prediction of the behaviors of fiber reinforced composites are highly dependent on the quality of the initial geometry of the model. Micro-/meso-FE modeling of fiber reinforced composites is a powerful tool, which gives the direction and density of the fibers that determines the permeability of the reinforcement and the mechanical properties of the final composite. XCT provides an opportunity for a detailed examination of the inner structure of fiber reinforced composites, providing details of the composite microstructure, defect population, and damage distribution.[122-124] 3D images obtained by micro-CT can be used for a realistic modeling of composite materials. A range of researchers have predicted the properties of fiber reinforced composites based on the numerical models from XCT.[125-128] Some typical approaches of model generations for simulations are highlighted below.

A direct method based on X-ray tomography imaging has been widely used to determine FE models based on the real geometry of 3D reinforcements.[122-123,129] The separations of the yarns in different directions were usually specialized based on the homogeneity parameter. XCT-based meso-FE simulation of the transverse compaction of a 3D orthogonal reinforcement had been introduced using a hyperplasic model developed for fiber bundles. The deformation behavior of the yarns' geometry in the simulation was compared with real conditions as described in Figure 9.

A various segmentation approach based on micro-CT has been proposed by Jean Bénézech.[129] The geometric model was iteratively improved by a heuristic optimization process. The fidelity of the models with respect to the input μ-CT is evaluated using a measure of similarity including both gray levels and local directions. The approach allowed to build realistic numerical models of woven fabrics that preserved the prescribed weaving pattern and free of interpenetration of fiber, which made them compatible with numerical simulations. The flow chart of model generation is illustrated in Figure 10.

Liu et al.[124] proposed a statistical approach to generate the refine meso-scale representative volume element of 3D five-directional braided composites, which considered the fabric compaction and the axial yarn torsion. The method firstly extracted the regions of interest to obtain the reference model from the XCT data. Then, the geometric parameters of the collected yarns of reference model were statistically analyzed based on the scanning tomograms. Consequently, the meso-scale statistical model was reconstructed by fitting with the appropriate function. Figure 11 illustrated a statistical approach to generate the refine meso-scale representative volume element of three-dimensional (3D) five-directional braided composites based on XCTy data. The results showed the statistical model was capable of accurately presenting the effects of the fabric compaction and yarn torsion on the mechanical behaviors of 3D braided composites comparing with experimental tests. For textile structural composites, Represent Volume Elements (RVE) with realistic reinforcement architecture can
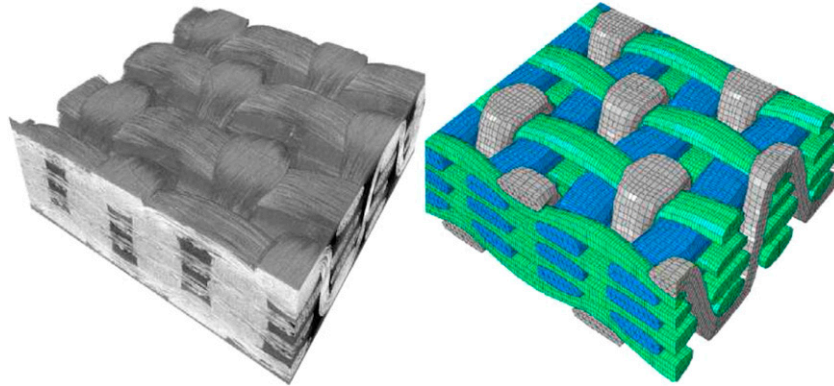
Figure 9. Comparison between the compacted tomography and the 3D orthogonal non-crimp woven simulation.[50]
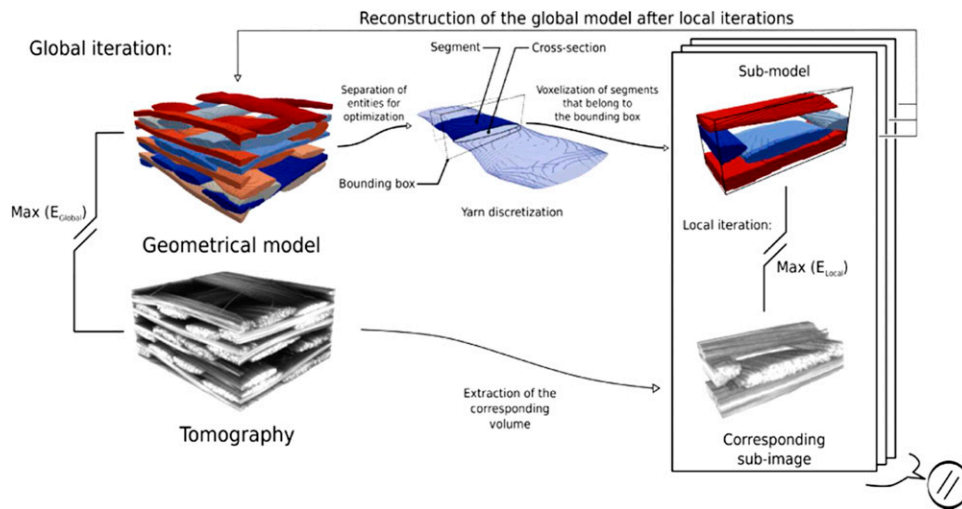

Figure 10. Schematic of the iterative global-local approach.[130]

obtain accurate predictions and identify the variability of mechanical properties. A data-driven modeling framework to generate statistically equivalent RVEs for three-dimensional orthogonal woven composites had been proposed.[131] The reinforcement geometry was characterized by Micro-CT in terms of fiber tow centroid coordinates and cross-sectional dimensions. The whole framework was described as in Figure 12 and any number of statistically equivalent RVEs can be generated for further simulations. Besides, a Monte Carlo algorithm for generating models of textile composites had been reported by R. G. Rinaldi.[132] Experimental data imaged using high-resolution XCT was used to establish target statistics. 3D solid tow generated by analogous algorithms represented geometrical models for more detailed failure analyses. Also, a voxel-based geometry reconstruction based on 3D woven composite CT scans had been proposed by B. Wintiba et al.[122] It

transforms explicit voxel RVE geometries into implicit smoothed geometries through a level set-based processing in Figure 13. During the post-processing, the yarns interpenetrations are suppressed, a thin gap is inserted between the contacting yarns and the fiber volume fraction is controlled locally by modifications of the yarns cross-section shapes. Then, a conforming tetrahedral mesh can be subsequently generated based on the implicit geometrical description for finite elements simulation.

Moreover, due to the high resolution of micro-CT, a fiber tracking algorithm to locate fiber centerlines from XCT has been used to generate micro-scale finite element models.[57] Three-dimensional images were obtained by fast synchrotron XCT scanning. A global overlapping stack filtering step was used followed by a local fiber tracking step. The new algorithm was found capable of efficiently defining fiber centerlines for the generation of micro-scale finite element
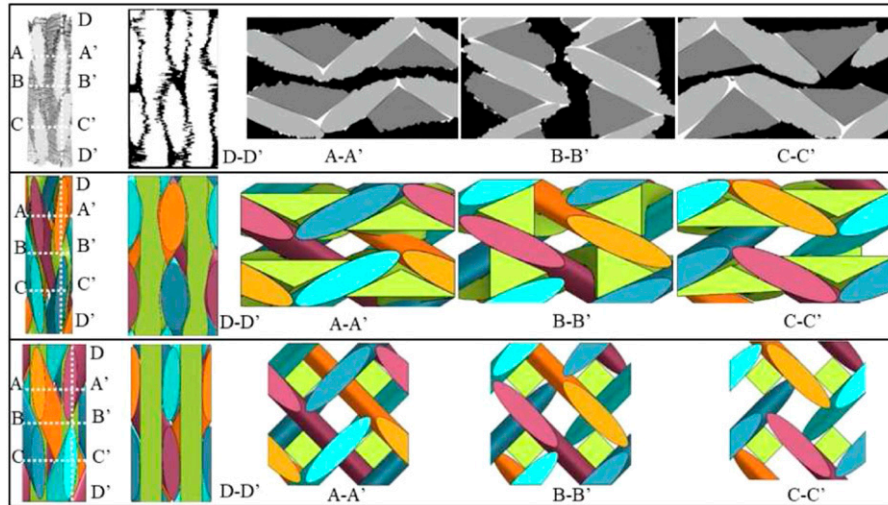
Figure 11. Comparison of the tomography for: the reference model, the statistical model, and the ideal model from top to bottom.[124]
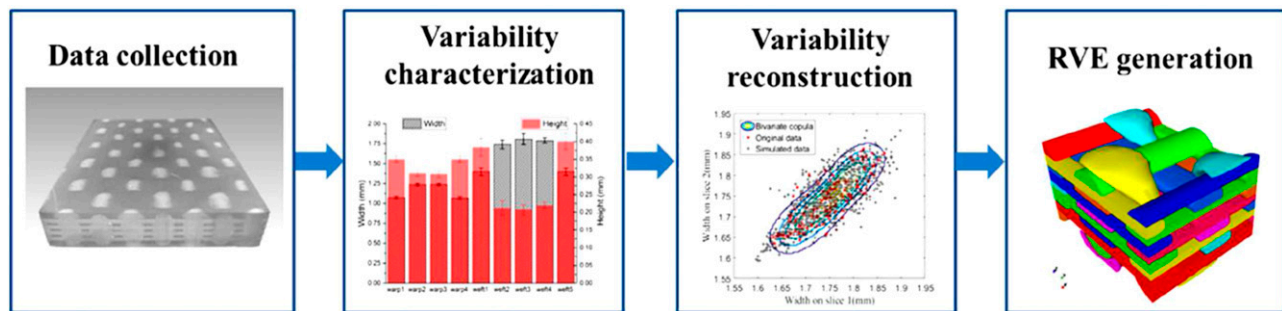

Figure 12. A data-driven modeling framework for generating statistical equivalent Represent Volume Elements.[131]

models with high fidelity. Figure 14 showed micro-scale finite element models from synchrotron XCT images for multidirectional carbon fiber reinforced composites.

3D CT images reconstructed from radiographs can also be used in DVC (and DIC) analysis.[53-54] The natural microstructural pattern distinguished by phase contrast is analogous to a speckle pattern. The accuracy of the DVC results could be improved by implementing a sub-voxel registration approach to achieve a resolution less than one pixel.

A detailed flow path analysis of a complex 3D woven angle-interlock fabric had been implemented by M.A. Ali et al.[45] using an in situ XCT experimental set-up. The resin flow path and reinforcement permeability in principle directions were predicted through vigorous digital flow simulations using computational unit cells extracted from the reconstructed 3D models from XCT scans. Figure 15 showed the flow paths through the fabric in X, Y, Z directions. The predicted permeability values were in good agreement with traditional benchmark experimental data, highlighting the utility of this novel technique.
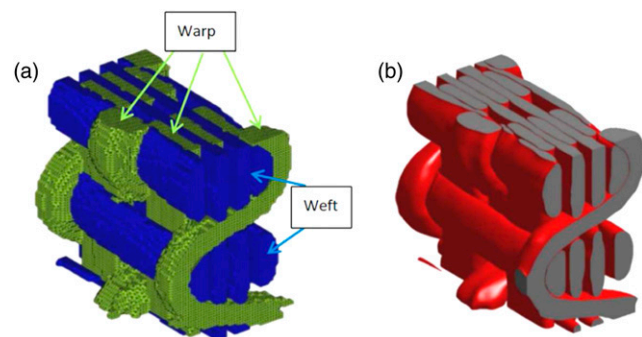

Figure 13. Voxel-based models. (a) Voxel geometry Represent Volume Elements, (b) Post-processed Represent Volume Elements.[122]

A comprehensive strategy for investigating the composite filter media with multi-scale complex structures using a combination of XCT and modular simulation models had
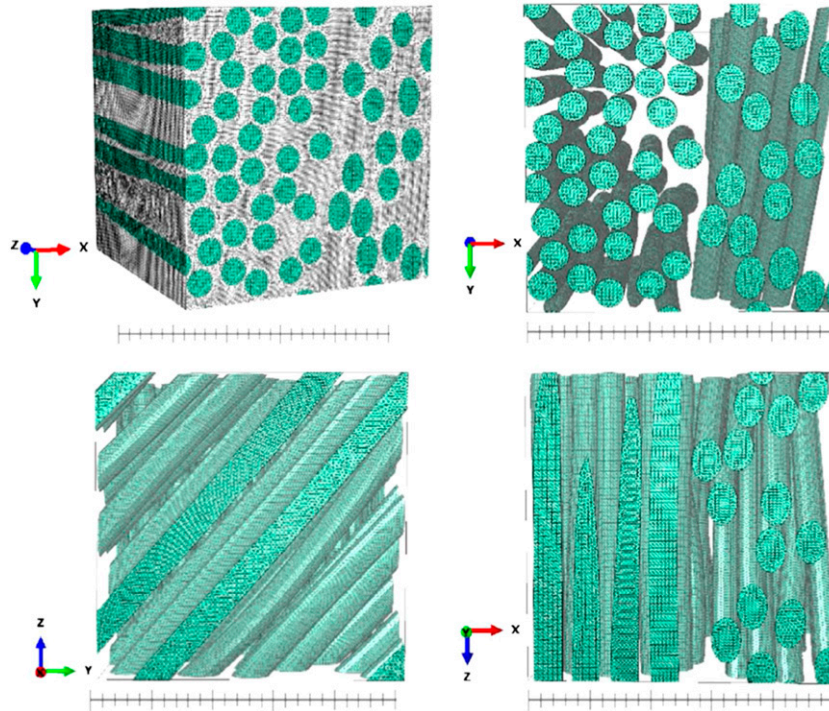
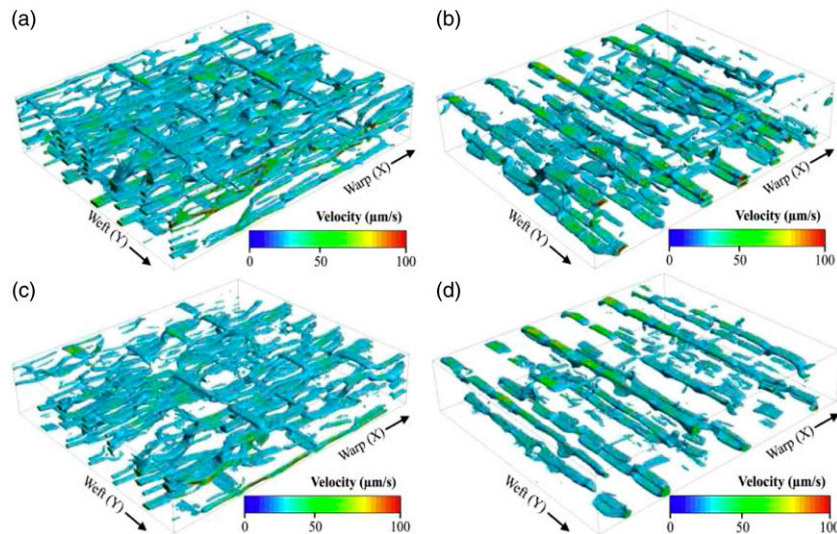**Figure 14.** X-ray CT image-based FE model by reconstructing fiber centerlines.[57]

Figure 15. Flow fields showing flow paths through the fabric[45] in (a) x-direction at h1, (b) y-direction at h1, (c) x-direction at h3 and (d) y-direction at h3.

been presented by Pan et al.[133] A 3D digital model of nanofiber-based filter media was reconstructed based on the X-ray tomography data for the cellulose substrate. Filtration simulations utilizing these models were conducted considering the drag force, Brownian diffusion, and aerodynamic slip. Figure 16 showed the reconstructed Virtual substrate and velocity field for air flow. Besides, XCT-based

models have also been used in moisture diffusion simulation of 3D textile composite materials.[125]

Microstructure characterization. Fiber-scale architecture (fiber arrangement in cross-section, 3D fiber waviness pattern, contacting frequency between fibers, etc.) has received great
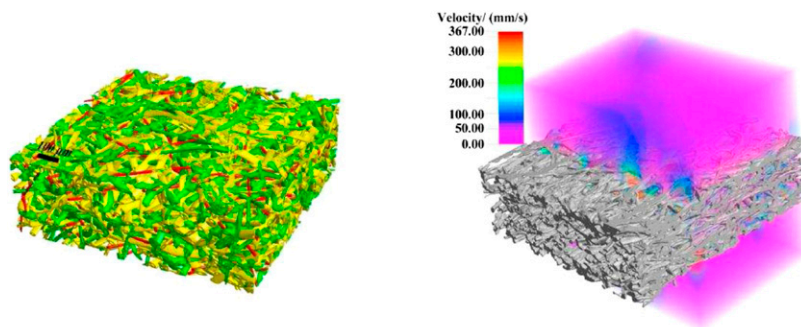
Figure 16. The reconstructed virtual substrate and velocity field for air flow through the reconstructed substrate from CT slices at a given flow velocity of 5.35 cm/s.[133]
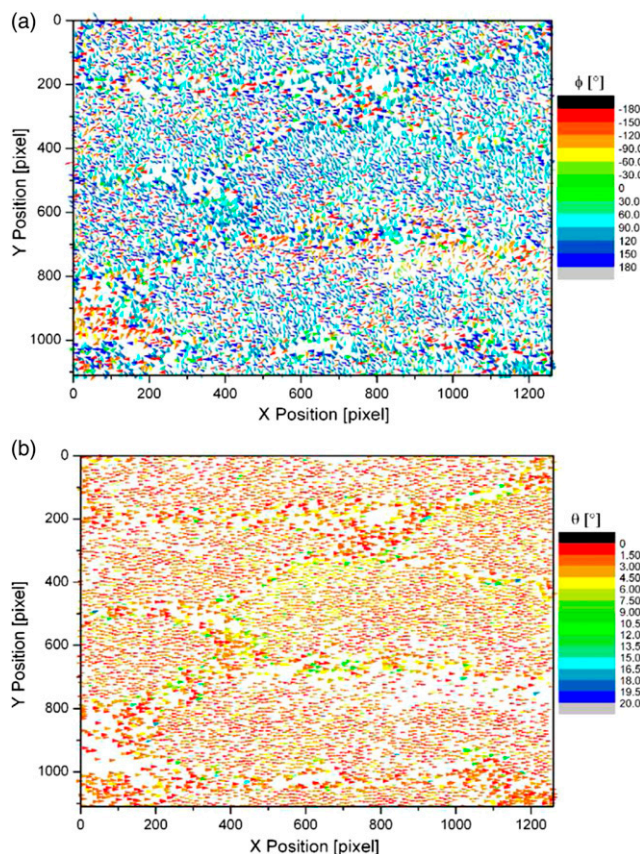

Figure 17. Orientation of the fibers in one slice.[10]

attention because it had a strong impact on the overall performance of the composite. As a non-destructive tool, X-ray CT can provide unrivaled advantages for the quantification and detailed mapping of microstructure and defects/voids as its high resolution in 3D imaging. Requena et al.[10] investigated the orientation of fibers (as showed in Figure 17) throughout the scanned volume of UD CFRP and located the largest misalignment within the channels separating fiber bundles from high-resolution XCT data. Fast et al.[11] derived complete

descriptions of the stochastic positions of each fiber in large bundles within CFRP based on synchrotron X-ray computed tomography (SXCT) data. Yu S. et al.[21] quantified the 3D microstructure of short basalt fiber-reinforced polyamide 6,6 composites (the fiber length, orientation distribution) by an XCT-assisted analytical measurements using the reconstruction models, as described in Figure 18. Yu X.W. et al.[25] proposed a method to quantify the variation of yarn fiber volume fraction of textile composites. Average fiber cross-sectional areas were acquired by analyzing hundreds of fiber cross-sectional areas in scanning electron microscopic images. Yarn cross-sectional area was determined by fitting ellipse to the labeled yarn cross-section in slices of micro-computed tomography images. Besides, there were many studies referring to analysis of fiber misalignment, spatial distributions, and hence volume fraction in textile structural composites.[15,23-25] Liu et al.[15] studied on 3D spatial distribution of steel fibers in fiber reinforced cementitious composites through micro-CT technique. The curves of fiber orientation distribution and fiber spacing distribution in cementitious composites were obtained and the orientation factor and dispersion coefficient of fiber were also determined.

Besides, a great deal of work has been done to extract the morphology and distribution of voids/defects by 3D volume rendering of the segmented void volume.[31-33,134] Kastner et al.[135] observed that the voids were mostly spherical in CFRP samples prepared by 20 layers of PREPREG C 970/ PWC T300 3K UT (TY) with relatively low void content, whereas in high-porosity specimens the voids tended to be flat and larger. The voids were not uniformly distributed. Sisodia et al.[49] correlated local void size and spatial distribution with fabric weave and resin infusion directions using high-resolution XCT. Manufacturing-induced defects such as fiber misalignment and porosity in a glass/polyester pultruded composite profile were characterized by Baran et al.[24] As shown in Figure 19, resin-rich areas were observed in between the glass rovings at which the unidirectional fibers were misaligned with respect to the desired pulling direction. Different types of porosities can be quantified and fiber
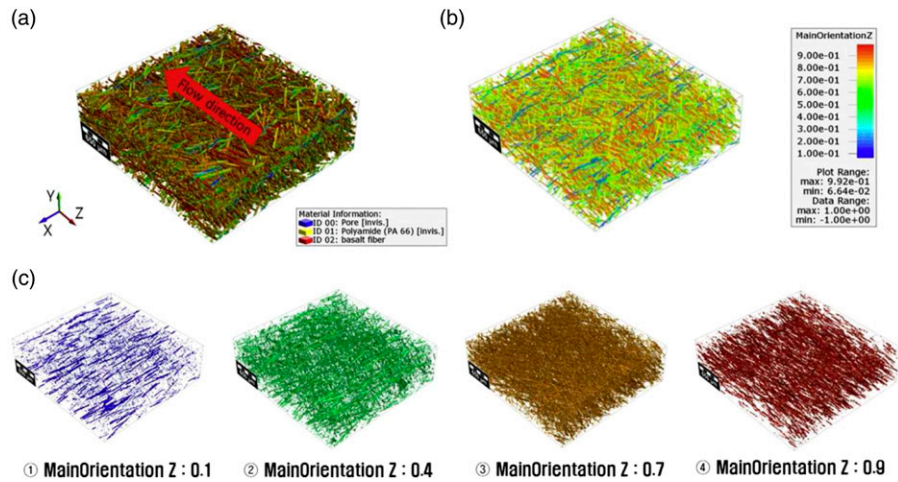
Figure 18. Internal microstructural characterization of the fiber orientation distribution.[21]
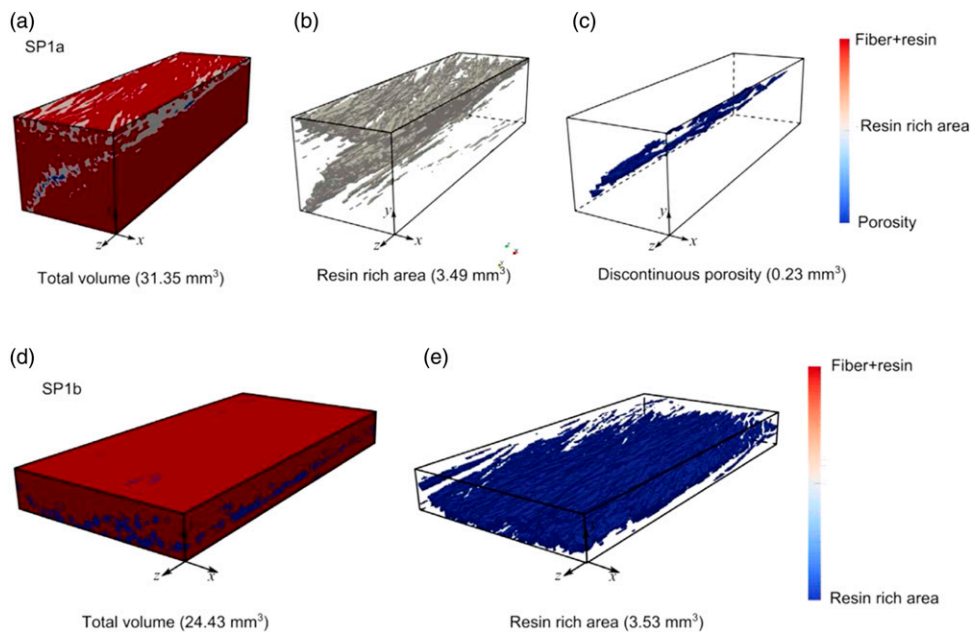

Figure 19. Representation of the voxel volume elements.[24]

misalignment was evaluated. Gao et al.[16] investigated the voids in 2D woven and 3D braided SiC$_f$/SiC composites by SXCT. The phases (fiber, voids, and matrix, as shown in Figure 20) were clearly observed and the 3D volume of voids were extracted. Figure 21 provided the 3D feature of pores in 3D braided SiC$_f$/SiC composite. The porosity in X, Y, Z directions was also calculated based on slices reconstructed from XCT data, as illustrated in Figure 22.

Assessment of manufacturing processes

The architectures and defects (misaligned fibers, pores, and resin-rich regions) in the composites, and even properties,

are strictly dependent on their manufacturing process. As a non-destructive tool, XCT can provide unrivaled 3D information to assess the quality of manufacture. Moreover, recent studies have started to emerge exploiting time-lapse imaging to follow the compaction of placed fibers/tows and textiles, the infiltration of the resin during the resin infusion process, the formation, transportation, and elimination of pores in the manufacturing and so on.

Compaction and densification characterization. In liquid composite molding (LCM), the compaction characterization of fibrous reinforcements plays a key role in determining the thickness, fiber volume fraction, and shape. The compaction
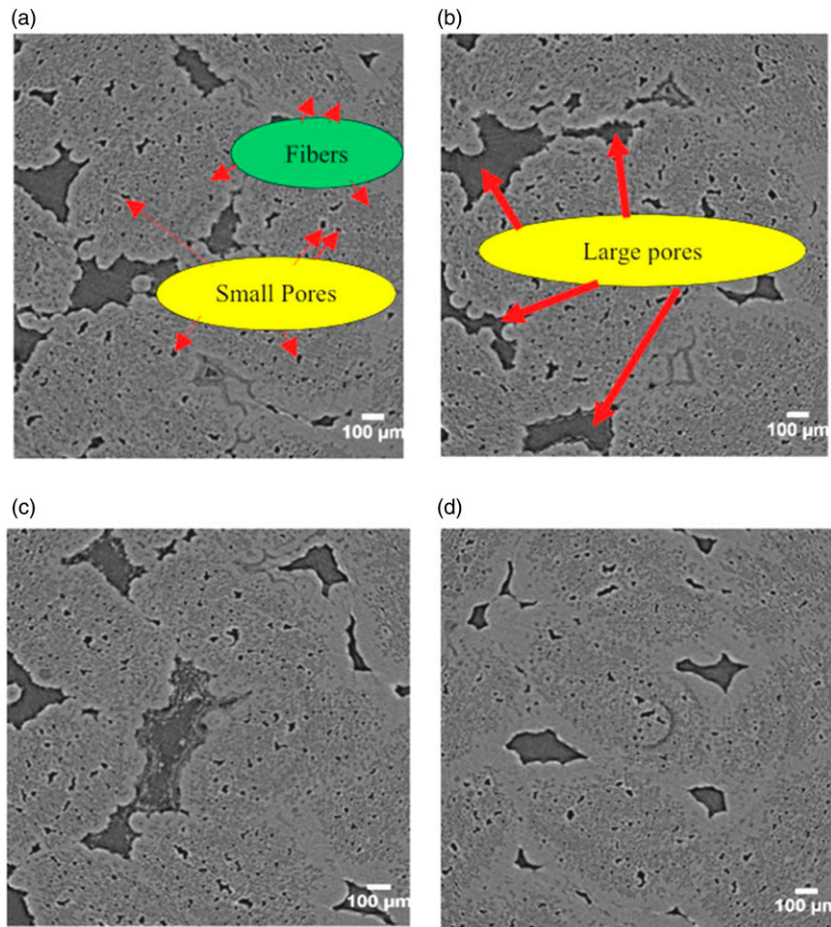
Figure 20. X-ray computed tomography images of 3D braided SiC$_f$/SiC specimen.[16]
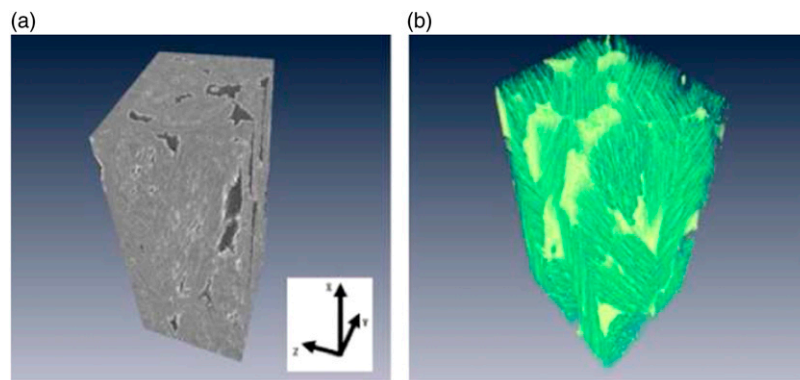

Figure 21. 3D volume images of (a) 3D braided SiC$_f$/SiC specimen reconstructed from the radiographic images and (b) pores extracted from the reconstructed volume of the composite.

response of three different types of 3D woven carbon fiber reinforcements, namely, orthogonal, angle-interlock, and layer-to-layer had been carried out by XCT as showed in Figure 23. Single-step, multistep, and cyclic compaction experiments were conducted. XCT analysis showed significant permanent deformation of z-binder yarns through the thickness of the reinforcements. The experimental data had been used to validate the model results.
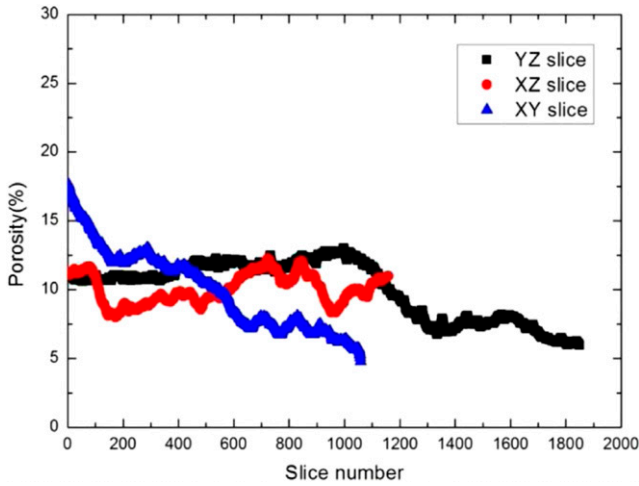
Figure 22. Porosity of specimen calculated from the sliced images in X, Y, Z directions.[16]

Non-crimp unidirectional (UD) fibers oriented and laid-up in one or multiple directions are dominant in fiber reinforced composites. Figure 24 described the evolution of the microstructure of a bundle of fibers subjected to a compression loading by using XCT. The compression induced both the bundle consolidation and liquid phase migration. In addition, the position, the orientation, the displacement, and the deformation of each fiber together with the position and the evolution of each fiber-fiber contact were followed during the compression. The result showed that XCT had detected the deformation behavior of fiber reinforcement effectively in manufacturing process of fiber reinforced composites.

In LCM of laminate, the effect of temperature cycle on the void volume fraction, shape, and spatial distribution was determined using X-ray microtomography. Cure temperatures were designed to obtain different processing windows while the overall degree of cure was equivalent, leading to
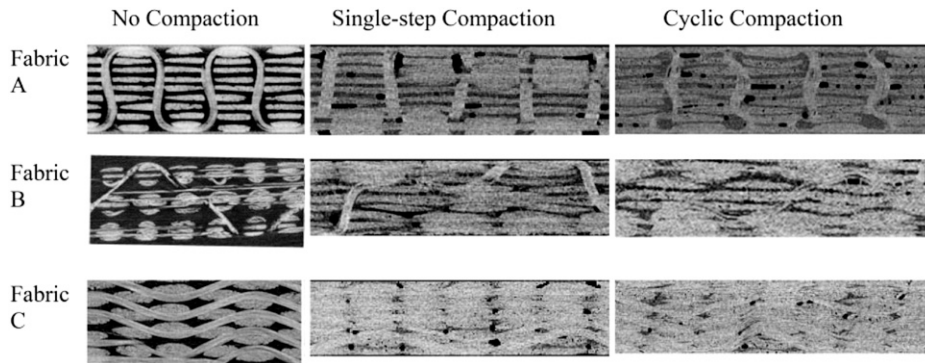

Figure 23. X-ray computed tomography scans of fabrics under different loading conditions.[38]
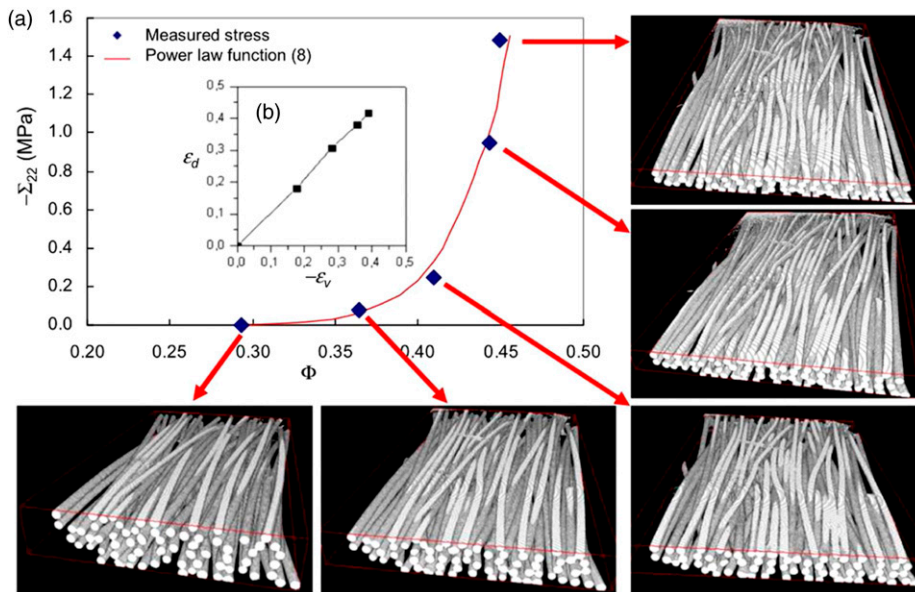

Figure 24. Mechanical response at the mesoscale: 3D segmented volumes obtained at the five compression steps.[39]

laminates with average porosities in the range 0.4%–2.9%, as showed in Figure 25. From XCT images, it can be seen that voids were elongated, oriented parallel to the fibers, and concentrated in channels along the width of the laminate.

Figure 26 showed densification process of C/C composite by CVI. Based on 3D images acquired by using high-resolution XCT, a computational tool for the modeling of CVI of carbon/carbon composites had been introduced.

Resin flow behaviors and permeability characterization. To better understand the relationship between manufacturing parameters and the introduction of defects, it is necessary to monitor the production of composite components. Some in situ vacuum-assisted infiltration experiments had been carried out using SXCT to study the mechanisms of microfluid flow within a fiber tow.[42-43,46-49] In Figure 27, it can be seen that SXCT is the capability to provide detailed information of microfluid flow and void transport in composite materials. Figure 28 represents the transverse flow perpendicular to the fiber tow captured simultaneously at three different locations. A high local fiber volume fraction was seen in the regions of high capillary pressure. Transverse flow was reduced in regions where local fiber volume fraction was high, which resulted in a decrease in permeability. Thus, it can seen that the in situ CT experiment had been successfully used to study the permeability behaviors of fluid in fiber reinforcement.

In situ XCT during axial impregnation of unidirectional fiber beds had been used to study to produce a high-quality product in a low impregnation time.[42] Figure 29 illustrated the flow behaviors through quasi-unidirectional non-crimp fabrics during resin infusion captured using in situ SXCT.
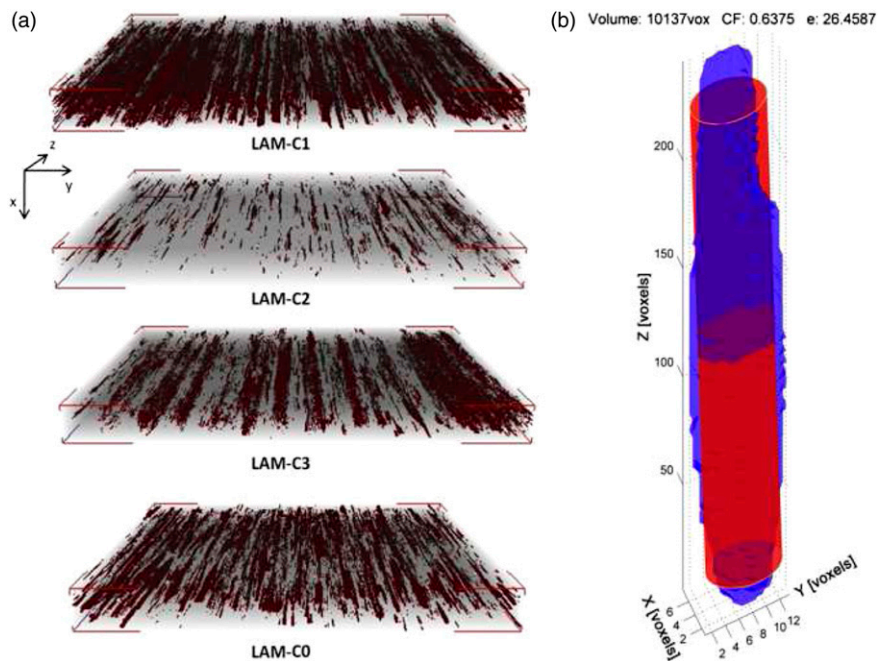

Figure 25. (a) X-ray microtomography of void spatial distribution in the composite panels (b) Typical rod-like void together with its equivalent cylinder.[33]
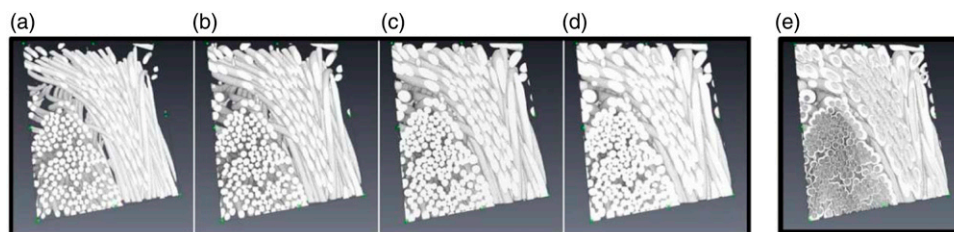

Figure 26. Densification of C/C composite (a-d) Four steps of the infiltration of a 400 × 400 × 350 voxels block; (e) Rendering of the deposited matrix.[136]

Finally, a low impregnation time had been achieved through a detailed XCT analysis of the fibrous preform by process optimization.

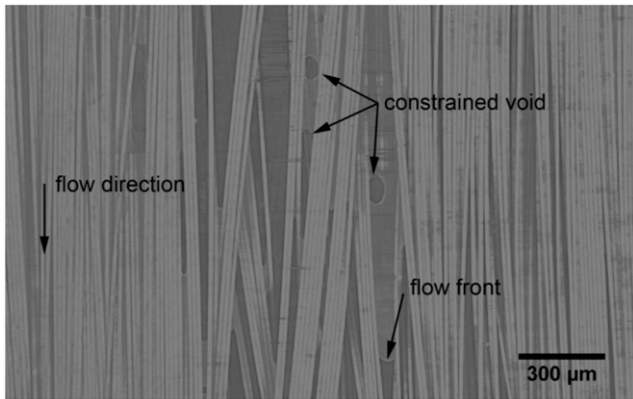Resin flow into dry reinforcement regions can result in microstructural change during the processing and influence air evacuation and void suppression. Such impregnation flow was investigated experimentally using XCT.[43] The experimental data was used to investigate the initial microstructure of the material and measure the extent of impregnation at each processing stage, the rate of impregnation, and the evolution of macro-porosity within the material. Figure 30 provided voids reduction process at different infiltration time.

A detail review specially focused on XCT for the virtual permeability prediction of fiber reinforcements for LCM processes can be found in reference.[44]

Mechanical properties of the fiber reinforced composites

The XCT has wide applications on characterizations of mechanical properties of fiber reinforced composites, such as static mechanics (tensile, compression, flexure, torsion and so on), fatigue, and impact. Due to the heterogeneous nature, the failure process is complex and the damage mechanism is difficult to be exposed. In recent years, both
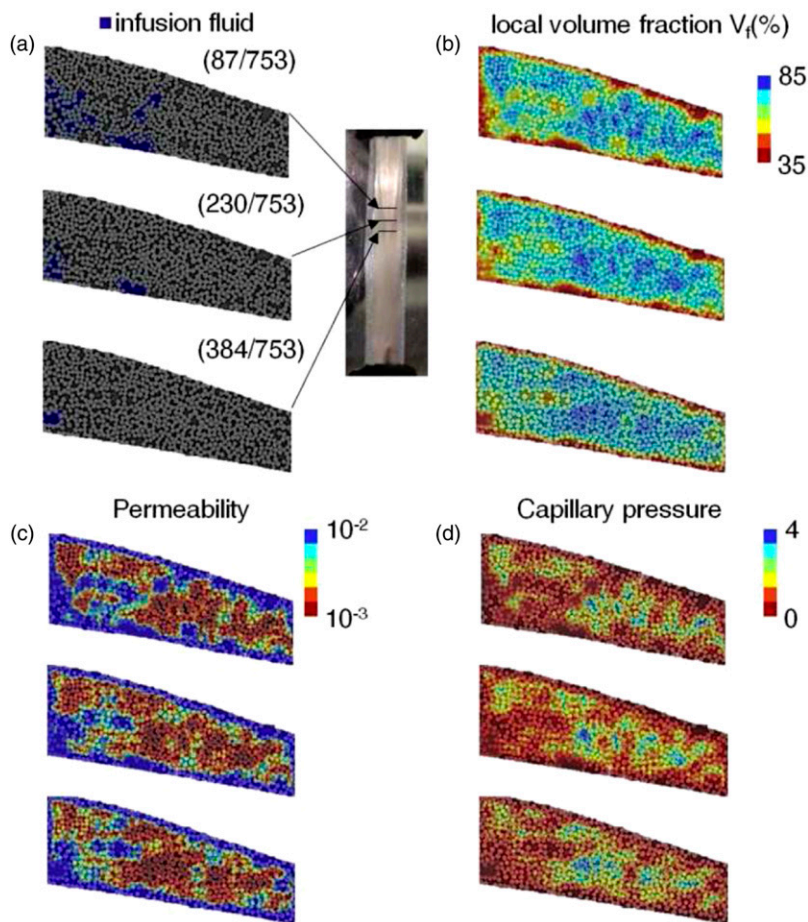

Figure 27. Longitudinal cross-section of the impregnated tow.[46]

Figure 28. In situ flow monitoring of the E-glass tow obtained from synchrotron X-ray computed tomography.[46]
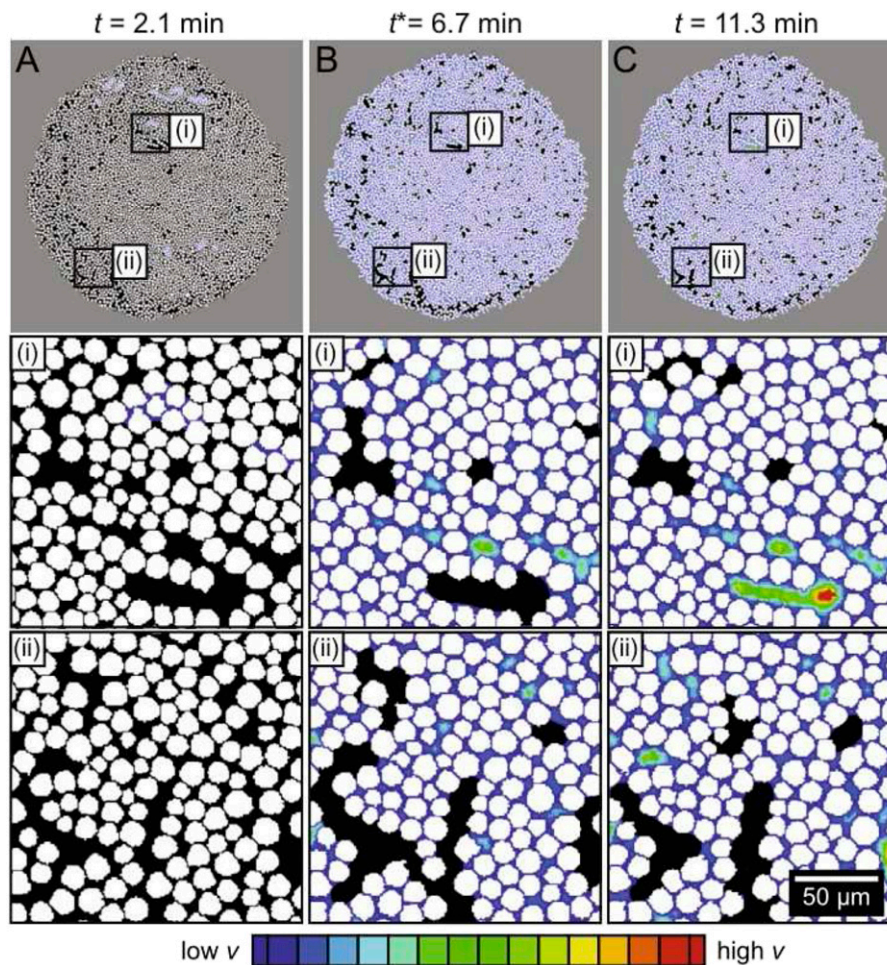
Figure 29. Pseudo-velocity maps for unsaturated flow.[42]

ex situ and in situ XCT in the area of materials have been rapidly developed and played a great role in elucidating fracture and failure mechanisms. Especially, high temperature in situ devices enhanced the damage and cracking mechanism research.

Static mechanics. Usually, mechanical loading modes consist of tensile, compression, flexure, torsion and so on. The specimen will show different failure mode as the loading is different. Many researchers had investigated failure mechanism of fiber reinforced composites at different loading type by means of XCT. Some typical studies were illustrated to highlight the capability of X-ray CT and the current state in this field.

Zhou et al.[70] investigated tensile failure and damage visualization based on progressive damage mechanics of three-dimensional braided composites by using Micro-CT imaging. As described in Figure 31, the specimen mainly

experienced the initiation and propagation of cracking and debonding but there are multiple damage mechanisms (matrix cracking, bundle cracking, matrix/yarn interfacial debonding, interface slip, fiber fracture, bundle fracture, and fiber pull-out) in the failed specimen. In addition, longitudinal cracks first developed along the path of the least resistance between yarns under low tensile stress, and transverse cracks initiate and propagate along a relatively straight path under high tensile stress. Scott et al.[72] carried out high-resolution computed tomography for carbon/epoxy laminates loaded in situ to failure. The experimental data allowed major damage mechanisms to be quantified in 3D, in an unambiguous and mechanically representative way. Figure 32 showed the matrix damage and crack growth process.

A XCT in situ shear test was designed to obtain micro-CT images of plain weave glass-fiber reinforced composite.[96] Damage evolution characterization of the plain
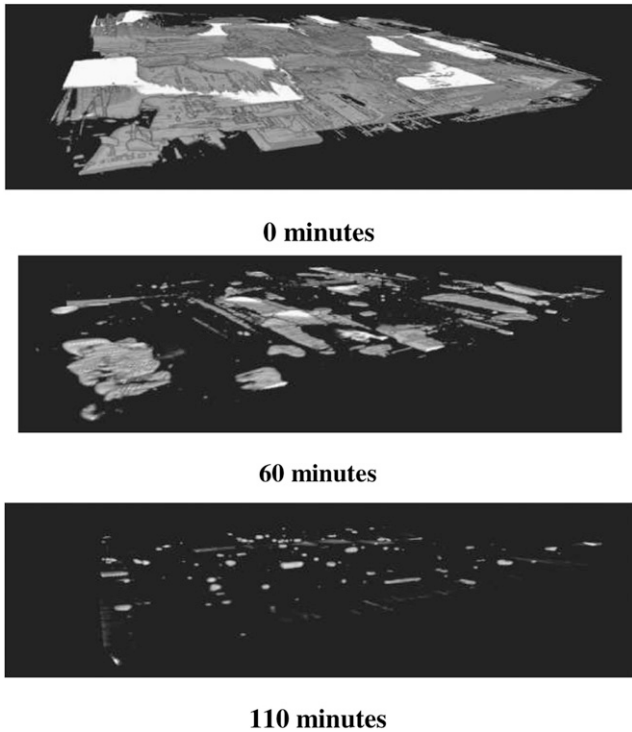
0 minutes

60 minutes

110 minutes

Figure 30. 3D renderings of void content, distribution, and morphology.[43]

weave glass-fiber composites under in situ shear experiment was realized by visualizing damages in 3D. Figure 33 showed the cracks distribution marked by using the image processing methods in all stages of in situ experiments.

With the aid of time-lapse SXCT and in situ loading, the real-time damage evolution in braided CFRP tube under torsion had been reported by Chai et al.[33] The result indicated progressive damage evolution under torsion initiated in the form of inter-tow debonding and intra-tow matrix cracking, followed by fiber micro-buckling and kink-band formation at tow cross-over points. The evolution of inter-tow debonding and intra-tow cracking had been quantified from XCT results. The initiation and propagation process of inter-tow debonding and intra-tow cracking under torsion was shown in Figure 34.

In recent years, more and more work has been untaken on damage propagation by using in situ XCT.[71,137-139] Damage development has been observed in situ within a 3D needle-punched carbon fiber reinforced carbon and silicon carbide ceramic composite, as compressive loads were applied longitudinally, transversely, and obliquely to its anisotropic structure.[71] The result showed cracks existed within the microstructure before the application of load and their propagation was affected by the heterogeneous microstructure and the direction of loading, as described in Figure 35.

Furthermore, high-resolution XCT enables the accurate mapping and measurement of damage modes down to individual fiber breaks, intra-laminar cracks, and interlaminar delamination. Watanabe et al.[93] analyzed the crack initiation and propagation under the application of opening load using in situ SXCT with a spatial resolution of ∼50 nm. The results showed that the voids and cracks initiation were not only the result of local stresses but also due to fiber/plastic interface debonding and in-resin crack initiation, as shown in Figure 36. Voids (sub-μ m) often formed in front of the crack tip and merged with the propagating cracks. Nanoscopic SXCT provided indispensable information on these nanoscale mechanisms, which cannot be obtained with traditional methods, including macroscopic observations and mechanical theory. Wang et al.[101] resolved longitudinal splitting, matrix micro-cracks, and fiber failures associated with kink-band formation by X-ray CT in CFRP failed under compression in Figure 37.

Hu et al.[67] investigated the underlying micro-damage mechanisms of randomly oriented short fiber reinforced composites on the basis of real internal microstructure characteristics obtained by the high-resolution (0.7 μm/ pixel) SRCT experiments. The failure mechanisms of the two materials were studied by the quantitative extraction and analysis of microstructure parameters in high-resolution 3D images. The three types of fibers near fracture surfaces were clearly characterized in Figure 38. Also, a higher resolution (0.33 μm/pixel) in situ SXCT had been conducted to research on internal 3D strain evolution of a failure process on a short carbon fiber reinforced composite. The microstructure and strain value of the material were successfully analyzed simultaneously in 3D for the first time.

3D observations of damage evolution in materials in extreme environments had been a challenge. Also, relatively little work has been conducted on damage propagation in fiber reinforced composites at elevated temperature.[62-63] One notable study was that by Bale et al.[63] who have compared the tensile failure behaviors of two ceramic matrix composites at both room and elevated temperature as shown in Figure 39 by using the rig shown in Figure 6(a) mounted at the ALS. They had fully resolved sequences of microcrack damage as cracks grow under load at temperatures up to 1,750°C by using in situ CT experiment.

Fatigue. The most of fatigue studies on fiber reinforced composites had been conducted at the macroscopic scale to analyze the influence of damage accumulation on the degradation of the material properties. Recently, thanks to advanced non-destructive techniques such as XCT, attentions have been focused on micro scale with the aim of building up a micromechanical understanding. The most common approach used to observe fatigue damage
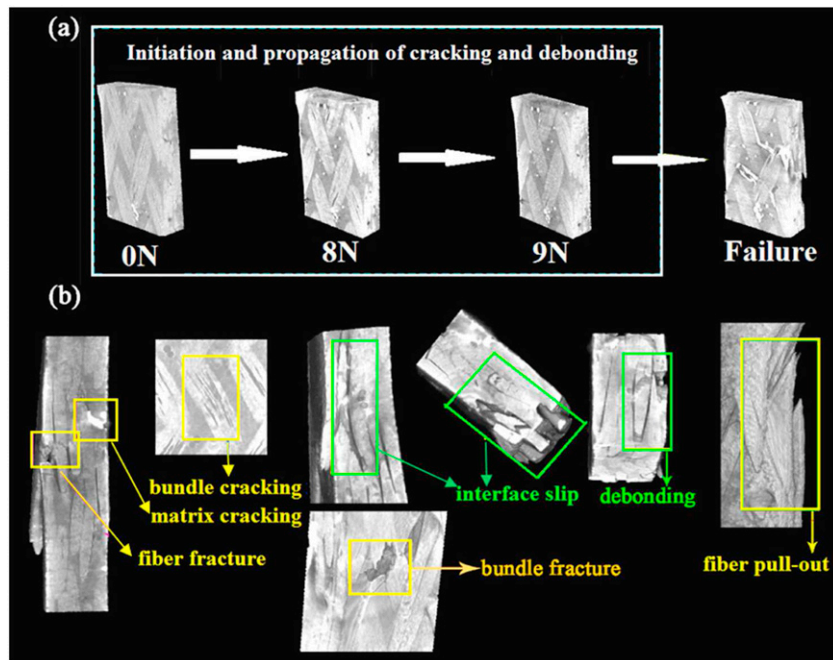
Figure 31. Micro-CT 3D volume and failure micrographs of the specimen.[70]
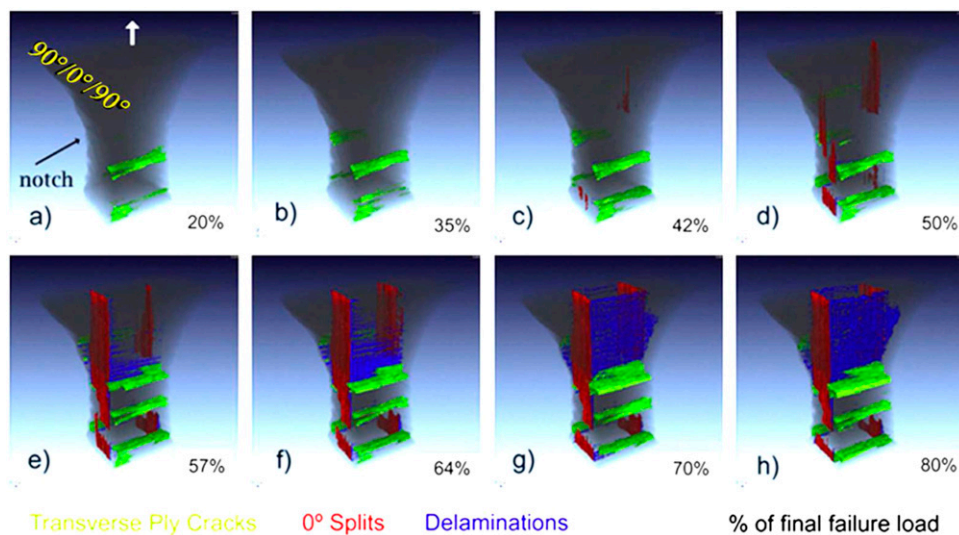
Figure 32. Matrix damage and crack growth: in situ loading from 20% to 80% of failure load.[72]

by XCT is to perform interrupted tests. Two main strategies have been applied: (i) the use of different specimens to investigate different loading conditions (load/cycles); (ii) the use of the same sample to monitor damage at different stages (same load and different number of cycles).

Many researches on fatigue damage development of fiber reinforced composites had been conducted by ex situ experiments.[65,140-141] Liu et al.[81] implemented an experimental investigation of tension-tension fatigue failure mechanisms in braided carbon/epoxy composites without/ with yarn-reduction subjected to different stress levels of ultimate tensile stress. Micro-CT was conducted to visualize and quantify the damage generated in the fatigued samples. The damage behavior was observed as shown in Figure 40. However, recently, in situ XCT imaging of fatigue damage

Figure 33. Crack marks at various stages of damage.[96]

Figure 34. 3D volume rendering showing initiation and propagation of inter-tow debonding (blue) and intra-tow cracking (red) as the shear strain is increased from 0 to 3.2%.[76]
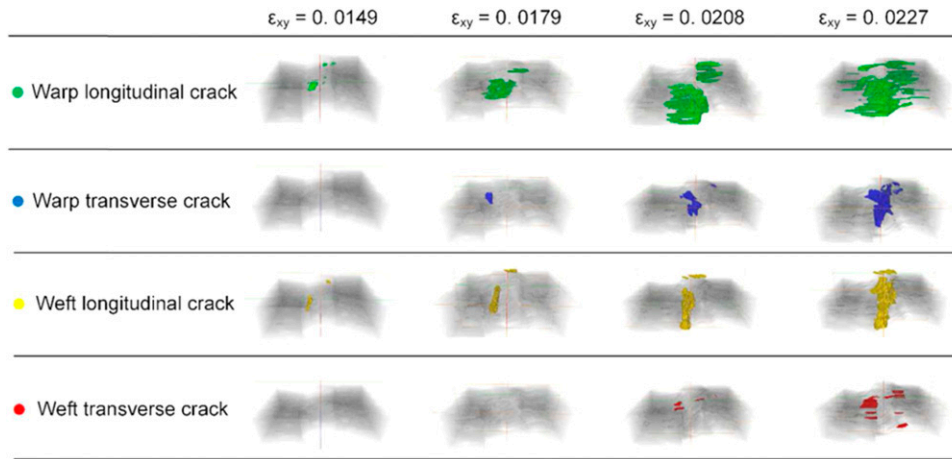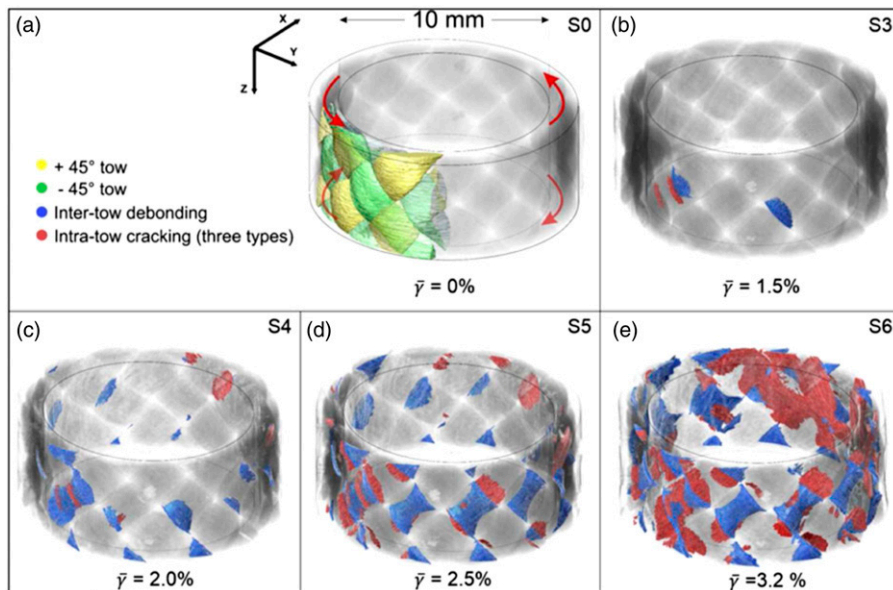
evolution has been widely performed by using both lab-XCT and SXCT. Garcea et al.[78] studied on the fatigue damage mechanisms in cross-ply CFRP by using in situ SXCT and the role of toughening particles in damage propagation was highlighted, as described in Figure 41.

A time-lapse interrupted fatigue test had been conducted for 3D woven glass fiber angle-interlocked samples using laboratory XCT by Yu et al.[82] The development of fatigue damage was followed. 3D rendering of fatigue damage with different types of cracks after (a) 60%, (b) 75%, and (c) 90% of the ultimate life was shown in Figure 42. Besides, in situ high temperature fatigue experiment (Traction-traction (R =

0.1) fatigue tests at 250°C) had been carried out by Pannier et al.[99] For the used samples, intra-tow matrix cracks along fibers on the external plies were the first damage form at the ply-scale. It also proved environmentally assisted fatigue tests on composite materials are feasible.

Moreover, the competing demands of sample size and resolution could be resolved by assessing a repeating unit cell. Some have applied a hierarchical approach using initially low-resolution XCT scans to identify regions of interesting (RoIs) to image at higher resolution. RoIs were physically cut from the sample, but the sample is no longer available for further time-lapse observations. Withers
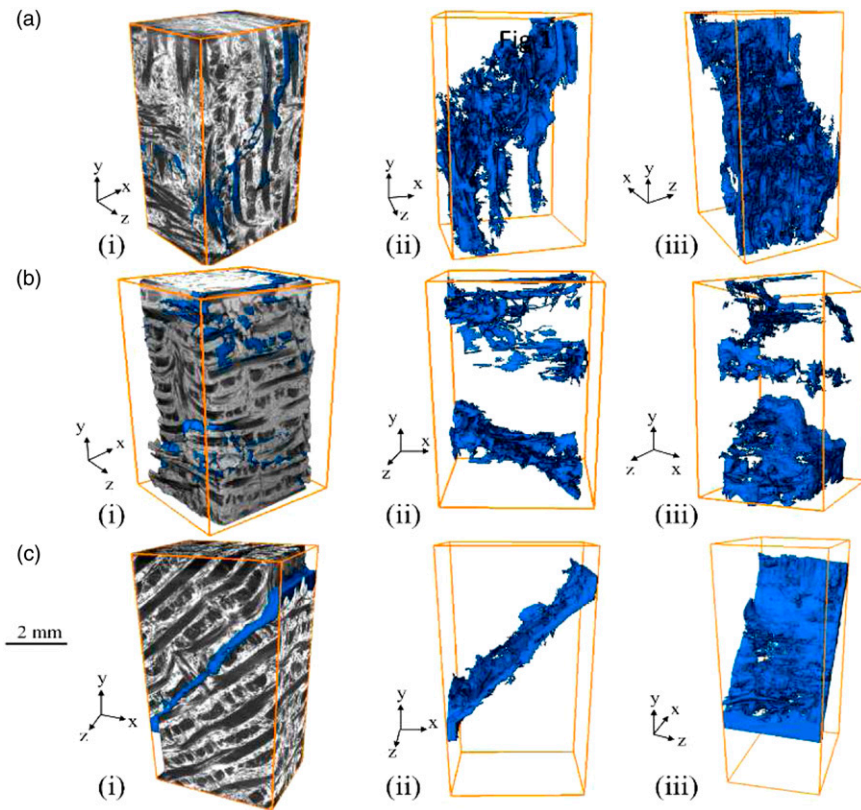
Figure 35. Tomography visualizations after testing for (a) longitudinal; (b) transverse, and (c) oblique loading orientations. The microstructure and major cracks shown in (i) and the segmented cracks shown from different viewing positions in (ii) and (iii).[71]
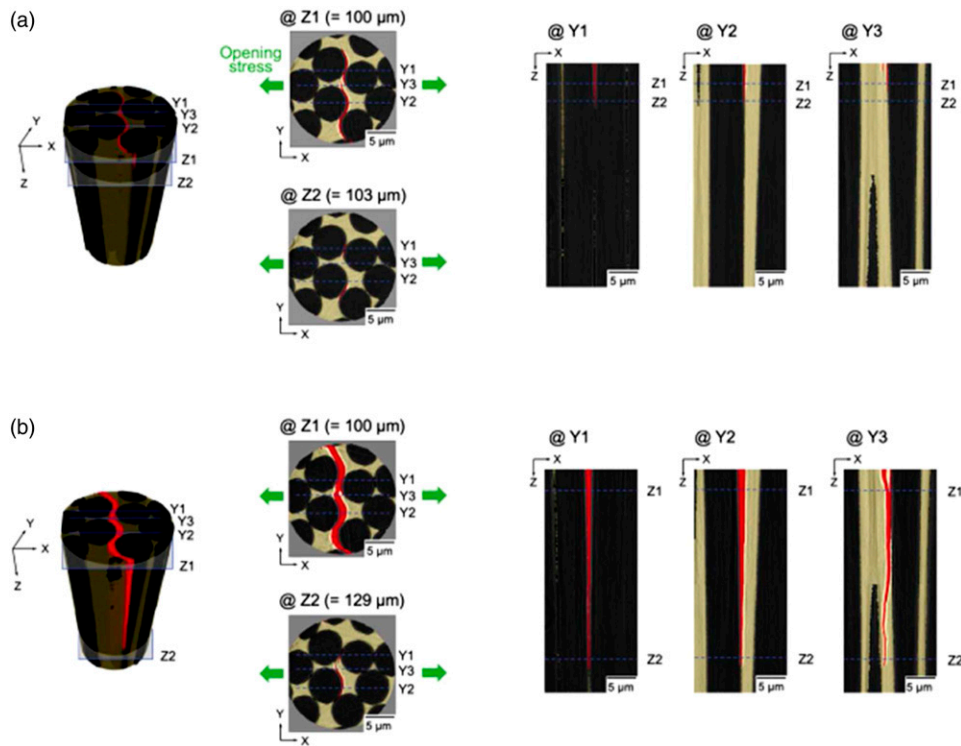

Figure 36. Crack initiation and propagation for the "thin"/"thick" resin region.[93]
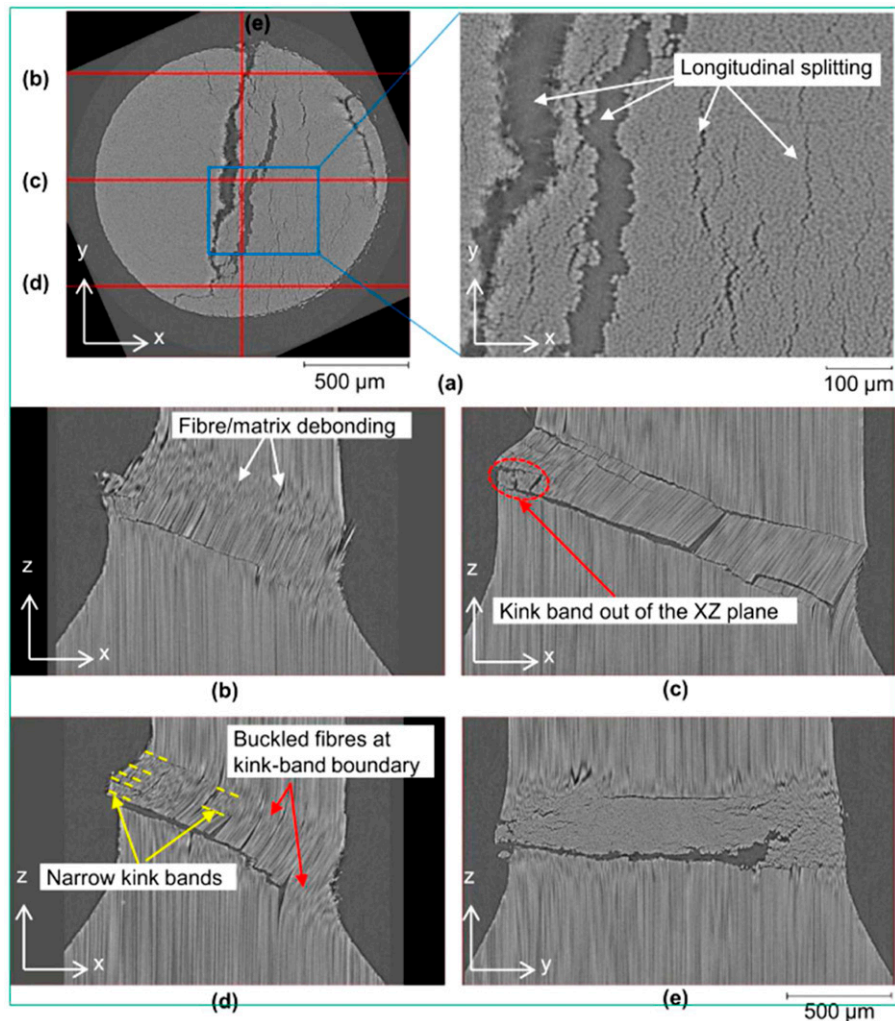
Figure 37. X-ray micro-CT virtual cross-sections of sample B: (a) XY, (b), (c) and (d) XZ, and (e) YZ, showing different views of kink bands inside the rod.[101]

et al.[141] have examined the bridging effect of the fibers in Ti-SiC fiber metal matrix composites. High spatial resolution X-ray microtomography was used to map the variation of crack opening displacement across matrix cracks. An alternative solution is to undertake RoI scans at higher resolution maintaining the integrity of the sample for further time-lapse experiments. Furthermore, it could be possible to study fatigue crack growth by crack inspection again and again after a certain number of fatigue cycles.

Impact. In terms of impact tests, exceptionally short durations and high strain rates are two special characteristics, which restrain the application of in situ X-ray CT imaging, especially in 3D. Therefore, XCT-based impact studies were generally confined to pre-test and post-mortem analysis. Another issue is that impact samples are conventionally thin

plates and the damage is often extensive. Usually, ROI and laminography are two effective ways in obtaining high-resolution images of impact-damaged regions.

In recent years, XCT imaging have been used to detect the damage behaviors of fiber reinforced composites in drop-weight and ballistic impact experiments.[87,142-146] Bull et al.[85] performed multi-scale 3D X-ray inspections, as shown in Figure 43, including micro-focus XCT and synchrotron radiation-computed laminography analyses of low velocity impact damage in CFRP. The lower resolution images indicated that the particle-toughening system suppresses delamination with very little effect on intralaminal damage. While the higher resolution images revealed that the particles contributed to toughening by crack deflection and bridging. The results revealed that in particle-toughened CFRP laminates, the particle-containing system restricted the propagation of
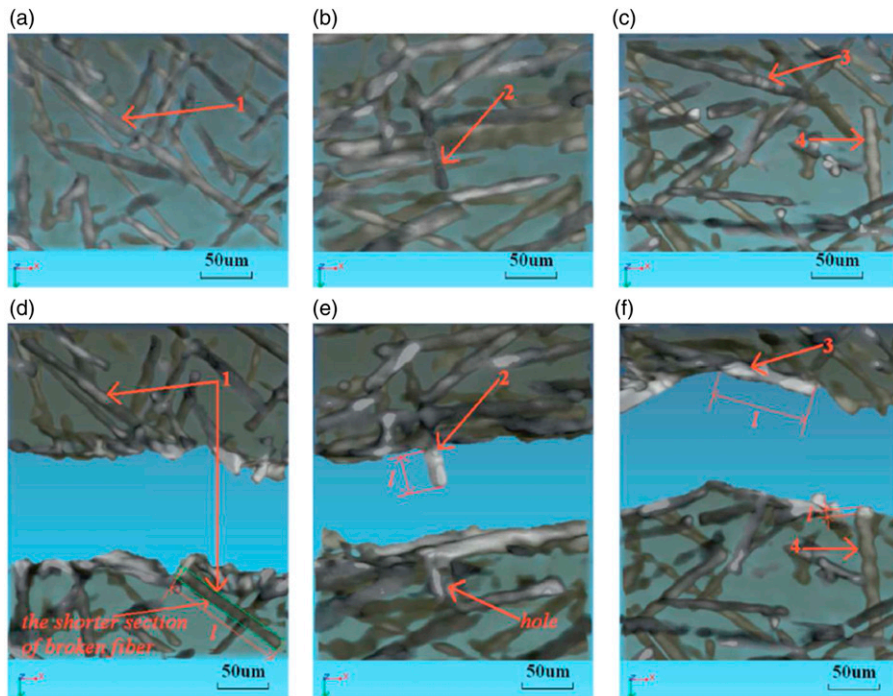
Figure 38. The three types of fibers near fracture surfaces.[67] Fiber 1 in (a) and (d) was broken into two sections. Fiber 2 in (b) and (e) and Fiber 3 in (c) and (f) are debonding fibers. Fiber 4 in (c) and (f) is a neighboring fiber.
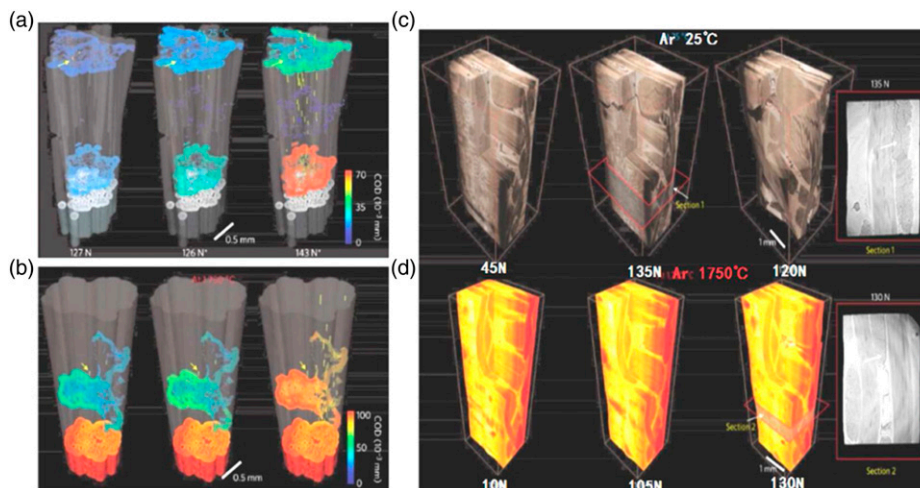
Figure 39. (a-b)Quantification of cracks in matrix and fibers of single-tow SiC/SiC composite (c-d) In situ tomography of C/SiC composite under tensile loads at 25 and 1750°C.[63]
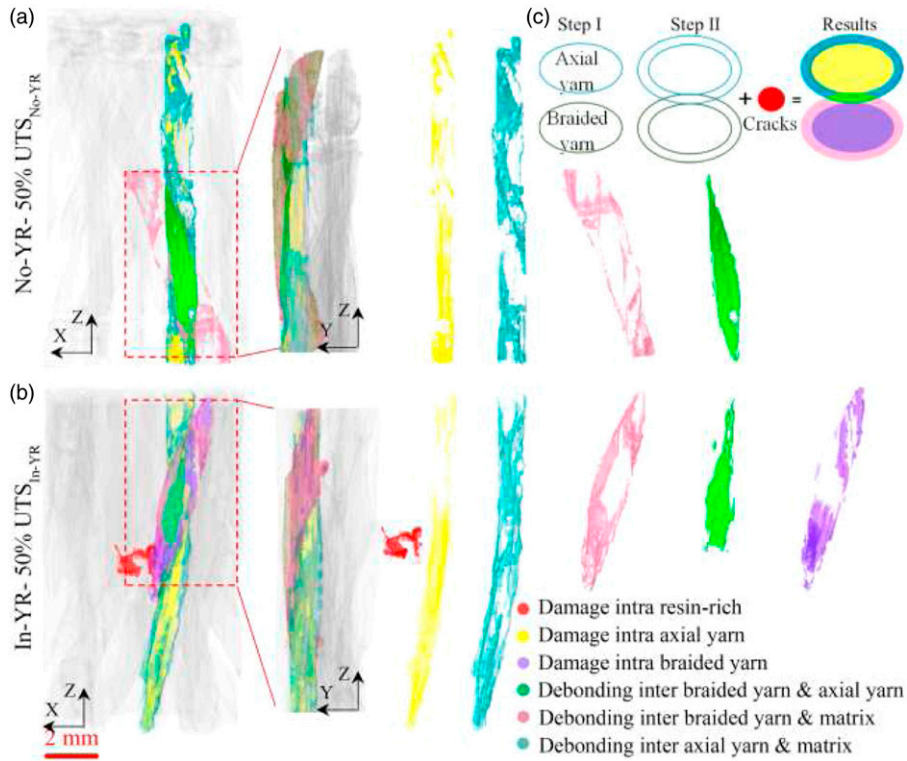
Figure 40. (a-b) 3D volume rendering of the damage showing the local damage distribution around the braided yarns and axial yarns of two types of samples, respectively, and (c) schematic diagram of two-steps damage classification.[81]
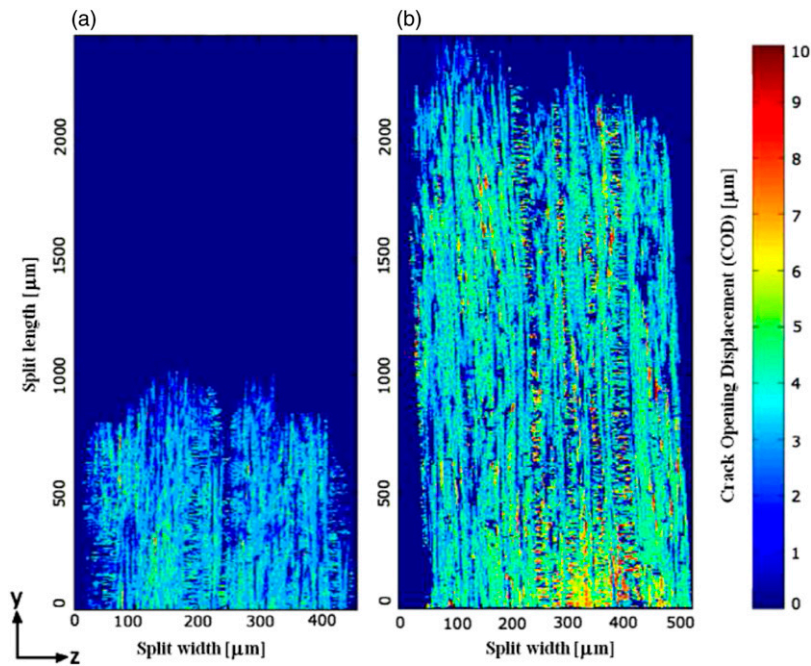
Figure 41. Fatigue crack opening displacement mapping for 0° ply splits at: (a) 30% σ_f and (b) and 50% σ_f (10^4 cycles).[78]
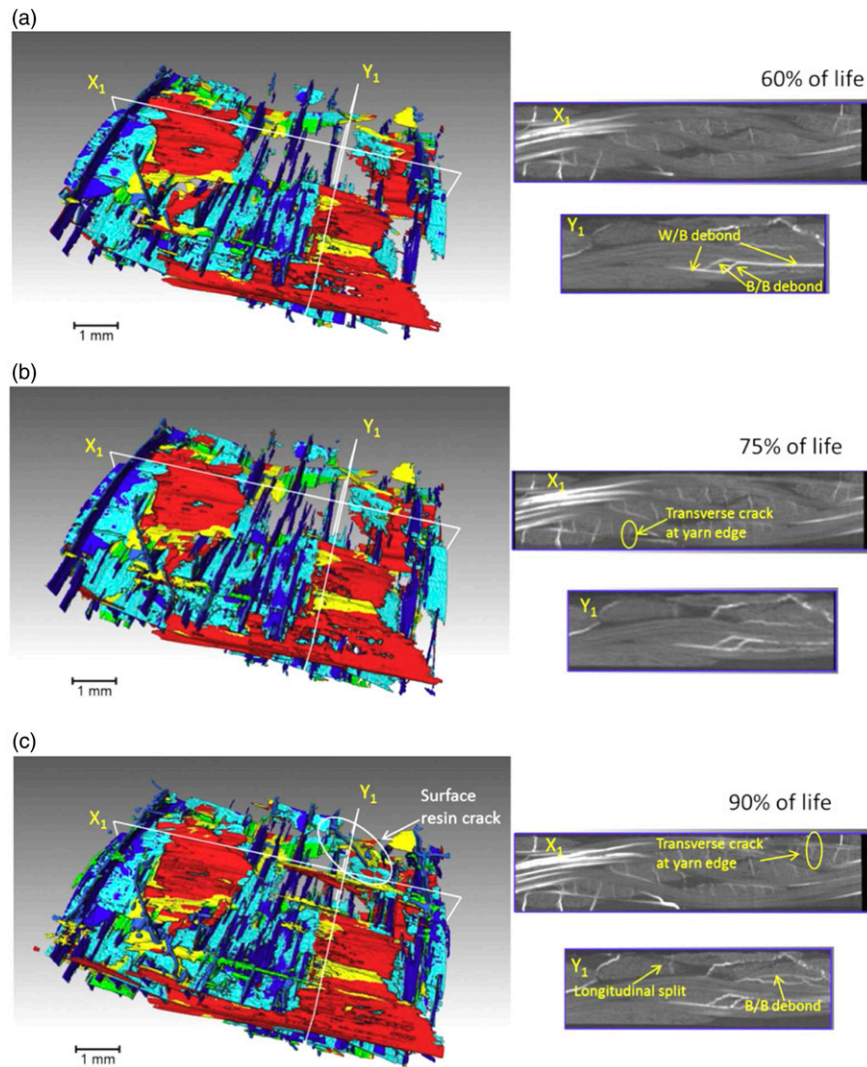
Figure 42. The damage after (a) 60%, (b) 75%, and (c) 90% of the ultimate life.[82]
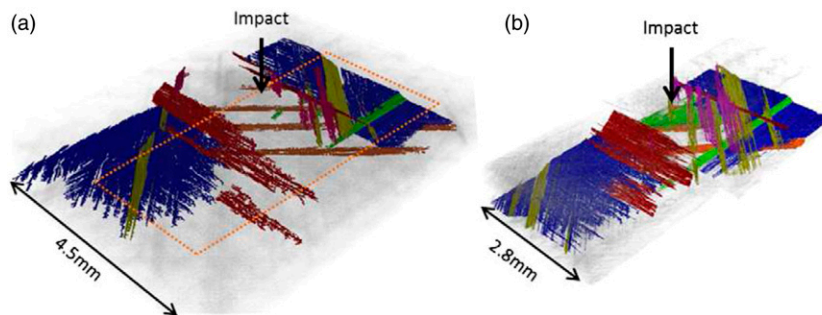
Figure 43. The damage morphology surrounding the impact region within the same specimen obtained by (a) μ-CT with the dotted region indicating the region obtained using (b) SRCT.[85]
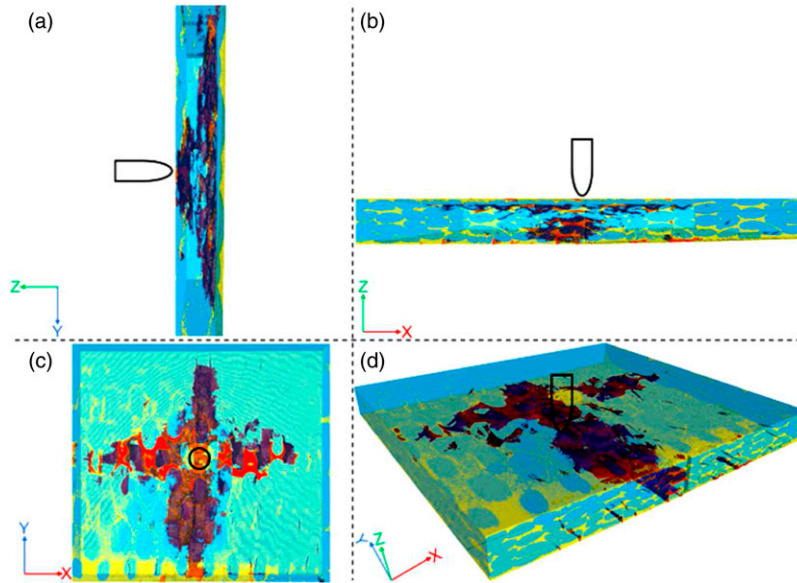
Figure 44. Spatial distribution of interface cracks in 3D angle-interlock woven composite subjected to 30J.[90]

delamination by inducing bridging and crack deflection. The impact and post-impact behaviors of CFRP laminates at various temperatures had also been studied using µ-CT. They found that specimens impacted at higher temperatures had reduced areas of delamination and increased residual flexural strength. Besides, crack deflection, fracture surface roughness, and bridging ligaments have all been quantified by analyses of XCT data. García-Rodríguez et al.[147] used X-ray analysis to detect internal impact damage in non-crimp fabric laminates. In addition, many other studies on damage mechanism of fiber reinforced composites, such as self-healing fiber reinforced polymers,[148] flax/glass hybrid composite,[86] and different textile structural composites,[149] had been conducted and the XCT imaging provided significant information on damage analysis, such as spatial distribution of interface cracks in 3D angle-interlock woven composite in Figure 44.[90] Also, the damage characteristics by XCT had been widely used to compare with predicted results to reveal the impact damage mechanism.

Physical and chemical behaviors of fiber reinforced composites

As we know, fiber reinforced composites have a wide range of applications in the fields of aerospace, defense, marine, nuclear and so on. Therefore, the material could face complex environments or conditions, such as moisture, corrosion, high temperature oxidation, and irradiation, in-
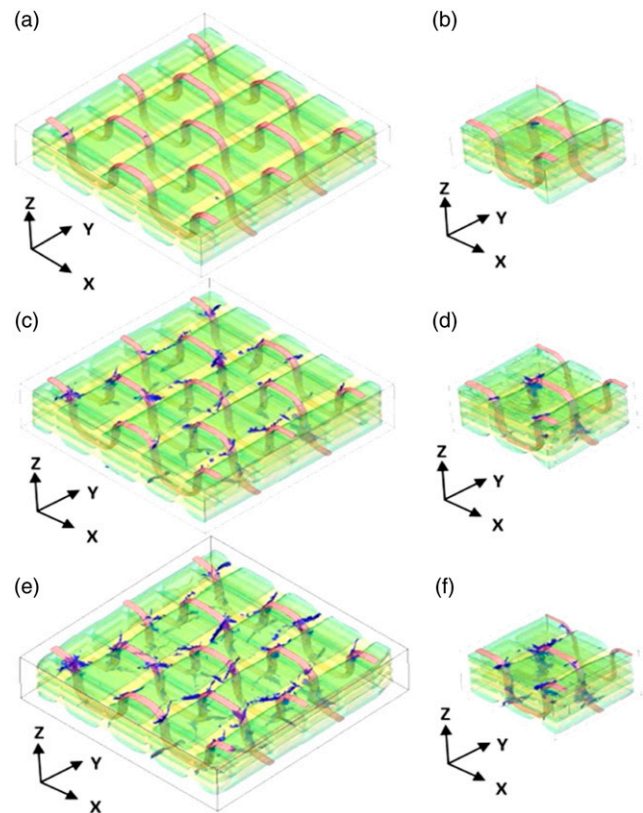
Figure 45. Comparison of cracking damage for "2 × 2 UC" (left), and "1 UC" (right) samples; (a) and (b) 200 cycles, (c) and (d) 800 cycles, (e) and (f) 1400 cycles.[104]
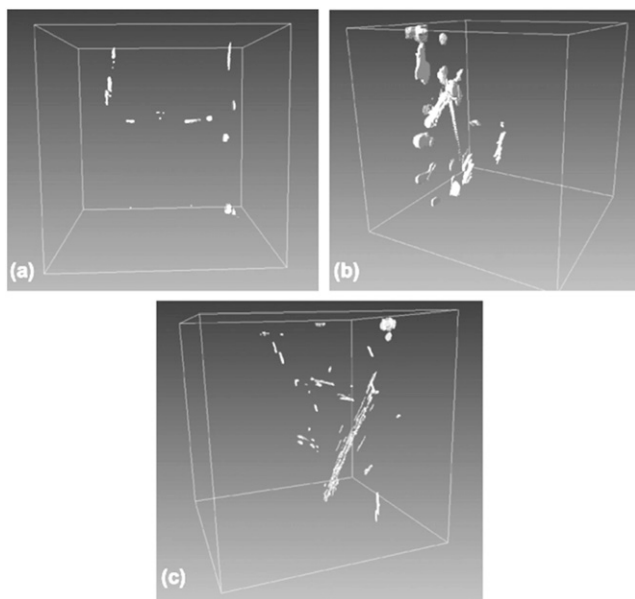
Figure 46. The distributions of the damage volume after UV treatments[110]. (a) 3D-glass (b) E-glass (c) carbon fiber.

service. XCT experiments can be conducted to detect the internal microstructure change under the environmental conditions. Gigliotti et al.[104] studied the thermal cycling behavior of 3D orthogonal woven composite. Qualitative and quantitative descriptions of the morphology and the evolution of cracks with thermal cycling were carried out through the analysis of μCT scans of samples at different cycle numbers. The crack development was described as in Figure 45.

C_f/SiC composites have been diffusely applied in aerospace engineering. Defects, are prone to occur in the fabrication process of C_f/SiC composites, which could lead to oxidative damage of components during service. The oxidation resistance of the material has been investigated by using CT imaging.[107] Besides, X-ray μ-CT had been used to detect inner structural damage of UV and heat-degraded polymer composites by Awaja et al.[110] Structural damage factors such as density change, reinforcement filler damage, homogeneity, cracks, and micro-cracks were examined. The distributions of the damage volume after UV treatments were extracted from CT imaging as shown in Figure 46.

Conclusions and opportunities

In the field of composites, these are both important attributes: the heterogeneity and complex 3D architecture of composite materials, while understanding the nucleation and evolution of defects is also critical to the structural

integrity. As a non-destructive characterization tool, XCT is superior in its ability to identify the internal microstructure of fiber reinforced composites, such as the complex 3D architecture of reinforcement from tow scale down to fiber scale, cracks in micro scale or even in nanoscale. Therefore, it has been widely used in modeling, microstructure characterization, and crack or damage observations in fiber reinforced composites.

For XCT 3D imaging characterization on fiber reinforced composites, of course, it is essential to perform multi-scale imaging for resolving from macro-to micro-scale/sub-micro-scale features in large composite structures as the competing demands between sample size and spatial resolution. Usually, the resolution used depends on the features we want to observe, for example, to detect the carbon fiber (diameter: 5–7 μm) or crack initiation, the high resolution of (<1 μm) is needed. Both laboratory X-ray CT system and Synchrotron X-ray CT facility can meet the requirements. However, some challenges still remain for the application of XCT to the study of composites. For synchrotron X-ray imaging, the required sample size is rather small compared to composite architectures and components, also limited access to users. On the other side, although laboratory XCT allows bigger components to be studied, images of composites can suffer from poor phase contrast and long acquisition times. Actually, laboratory X-ray CT and Synchrotron X-ray CT can be mutual complement. More recently, the imaging speed and the ease-of-use in-service are continued being improved. However, in order to assess very fast phenomena, such as impact damage, the temporal resolution needs to be further enhanced.

Thus, although a considerable amount of information can be obtained from a 3D image of a composite, a time series of 3D images is necessary in many cases, for example, resin flow in LCM, crack propagation under loading to deepen the understanding of composite materials regarding processing or in-service degradation. Recent 10 years, a sharp increase in 4D (3D + time) imaging had seen and they enable us to identify the nucleation, growth, and interaction of crack as a function of loading non-destructively. Also, such time sequences are useful for validating analytical or numerical composite models. Usually, there are three types of time series imaging, namely, ex situ, interrupted in situ, and continuous in situ imaging. SXCT can offer a wider range of flexibility in performing experiments, particularly when a certain level of phase contrast and/or high temporal resolution are required. In the *In situ experiments* section, some typical in situ devices had been listed for 4D imaging. The availability of smart loading devices designed for X-ray CT imaging, which are sufficiently compact and lightweight to be accommodated on the scanner, offering almost unimpeded views of the sample to X-rays, and stable even at the high rotational speeds needed for fast imaging, have enabled

the investigation of composite behavior in realistic service environments using in situ experiments or time-lapse studies. Consequently, unique insights can be obtained from time-lapse X-ray CT regarding processing or in-service degradation.

Besides, to distinguish phases and improve the detection of damage in composites, high resolution, staining with heavy elements, phase contrast, and holding cracks under superimposed loading had been explored. Now, the resolution has been improved significantly, allowing the observation of fiber-matrix debonding, and constituents with similar densities to be distinguished using phase contrast approaches. Moreover, synchrotron XCT faculties exploiting high flux and high brightness beams along with fast acquisition detectors and data transfer approach have enabled ultrafast continuous streaming, able to capture processes in real time.

To sum up, the progress gained in the last decades in XCT imaging has directly benefitted many applications in the field of composites. XCT is extensively applied to capture the geometric features inside the material, to track processing and to record the damage process. The images obtained by XCT scan experiments are also applied to analyze the manufacturing defects and extract geometric parameters to create different modelings. The in situ time-lapse CT data provides a basis for the analysis of material damage evolution, and the generation, distribution, and evolution of cracks. It is expected that the use of XCT will aid the developments of the fiber reinforced composites.

Declaration of conflicting interests

Funding

ORCID iD

Yantao Gao (iD) https://orcid.org/0000-0002-3479-1512

References

1. Lubin G. *Handbook of composites*. New York, NY: Van Nostrand Rheinhold, 1982.
2. Chawla N and Chawla KK. *Metal matrix composites*. New York, NY: Springer, 2014.
3. Bansal NP and Lamon J. *Ceramic matrix composites: materials, modeling and technology*. Hoboken, New Jersey, NJ: John Wiley & Sons, 2014.
4. Chen CH and Cheng S. Mechanical properties of fiber reinforced composites. *J Compos Mater* 1967; 1(1): 30–41.
5. Little JE, Yuan X and Jones MI. Characterization of voids in fiber reinforced composite materials. *NDT&E Int* 2012; 46: 122–127.
6. Feng Y, Feng Z, Li S, et al. Micro-CT characterization on porosity structure of 3D C_f/SiC_m composite. *Compos A Appl Sci Manuf* 2011; 42: 1645–1650.
7. Vavrik D, Jakubek J, Kumpova I, et al. Dual energy CT inspection of a carbon fibre reinforced plastic composite combined with metal components. *Stud Nondestruct Test Eval* 2016; 6: 47–55.
8. Naresh K, Khan KA, Umer R, et al. The use of X-ray computed tomography for design and process modeling of aerospace composites: a review. *Mater Des* 2020; 190: 108553.
9. Dilonardo E, Nacucchi M, De Pascalis F, et al. High resolution X-ray computed tomography: a versatile non-destructive tool to characterize CFRP-based aircraft composite elements. *Compos Sci Technol* 2020; 192: 108093.
10. Requena G, Fiedler G, Seiser B, et al. 3D-Quantification of the distribution of continuous fibres in unidirectionally reinforced composites. *Compos A Appl Sci Manuf* 2009; 40: 152–163.
11. Fast T, Scott AE, Bale HA, et al. Topological and Euclidean metrics reveal spatially nonuniform structure in the entanglement of stochastic fiber bundles. *J Mater Sci* 2015; 50: 2370–2398.
12. Rosini S, Mavrogordato MN, Egorova O, et al. In situ statistical measurement of local morphology in carbon-epoxy composites using synchrotron X-ray computed tomography. *Compos A Appl Sci Manuf* 2019; 125: 105543.
13. Nguyen NQ, Mehdikhani M, Straumit I, et al. Micro-CT measurement of fibre misalignment: application to carbon/epoxy laminates manufactured in autoclave and by vacuum assisted resin transfer moulding. *Compos A Appl Sci Manuf* 2018; 104: 14–23.
14. Stamopoulos AG, Tserpes KI and Dentsoras AJ. Quality assessment of porous CFRP specimens using X-ray Computed Tomography data and artificial neural networks. *Compos Struct* 2018; 192: 327–335.
15. Liu J, Li C, Liu J, et al. Study on 3D spatial distribution of steel fibers in fiber reinforced cementitious composites through micro-CT technique. *Constr Build Mater* 2013; 48: 656–661.
16. Gao Y, Wang Y, Yang X, et al. Synchrotron X-ray tomographic characterization of CVI engineered 2D-woven and3D- braided SiC_f/SiC composites. *Ceram Int* 2016; 42: 17137–17147.
17. Yan H, Li K, Gao Y, et al. Study on microstructures of 2D and 3D chemical vapor infiltration SiC/SiC composites. *Adv Eng Mater* 2020; 22: 1900880.

18. Tretiak I and Smith RA. A parametric study of segmentation thresholds for X-ray CT porosity characterization in composite materials. *Compos A Appl Sci Manuf* 2019; 123: 10–24.

19. Bale H, Blacklock M, Begley MR, et al. Characterizing Three-dimensional textile ceramic composites using synchrotron X-ray micro-computed-tomography. *J Am Ceram Soc* 2012; 95(1): 392–402.

20. Mehdikhani M, Straumit I, Gorbatikh L, et al. A dataset of void characteristics in multidirectional carbon fiber/epoxy composite laminates, obtained using X-ray micro-computed tomography. *Data Brief* 2019; 27: 104686.

21. Yu S, Hwang JY and Hong SH. 3D microstructural characterization and mechanical properties determination of short basalt fiber-reinforced polyamide 6,6 composites. *Compos B Eng* 2020; 187: 107839.

22. Wan Y, Straumit I, Takahashi J, et al. Micro-CT analysis of internal geometry of chopped carbon fiber tapes reinforced thermoplastics. *Compos A Appl Sci Manuf* 2016; 91: 211–221.

23. Sabuncuoglu B, Tanabi H, Soete J, et al. Micro-CT analysis of deviations in fiber orientation and composite stiffness near the microvascular channels embedded in glass-fiber reinforced composites. *Compos Struct* 2020; 237: 111896.

24. Baran I, Straumit I, Shishkina O, et al. X-ray computed tomography characterization of manufacturing induced defects in a glass/polyester pultruded profile. *Compos Struct* 2018; 195: 74–82.

25. Yu X-W, Wang H and Wang Z-W. Analysis of yarn fiber volume fraction in textile composites using scanning electron microscopy and X-ray micro-computed tomography. *J Reinf Plast Compos* 2019; 38(5): 199–210.

26. Hanhan I, Agyei R, Xiao X, et al. Comparing non-destructive 3D X-ray computed tomography with destructive optical microscopy for microstructural characterization of fiber reinforced composites. *Compos Sci Technol* 2019; 184: 107843.

27. Pickering KL, Bader MG and Kimber AC. Damage accumulation during the failure of uniaxial carbon fiber composites. *Compos A Appl Sci Manuf* 1998; 29: 435–441.

28. Zhang H, Genest M, Robitaille F, et al. *Infrared thermography, ultrasound C-scan and microscope for non-destructive and destructive evaluation of 3D carbon fiber materials: a comparative study.* Spie Sensing Technology+Applications. International Society for Optics and Photonics, 2015.

29. Trochu F, Ruiz E, Achim V, et al. Advanced numerical simulation of liquid composite molding for process analysis and optimization. *Compos A Appl Sci Manuf* 2006; 37(6): 890–902.

30. Chung Hae Park CH and Woo L. Modeling void formation and unsaturated flow in liquid composite molding processes: a survey and review. *J Reinf Plast Compos* 2011; 30(11): 957–977.

31. Hamidi YK, Aktas L and Altan MC. Three-dimensional features of void morphology in resin transfer molded composites. *Compos Sci Technol* 2005; 65(7–8): 1306–1320.

32. Mehdikhani M, Gorbatikh L, Verpoest I, et al. Voids in fiber-reinforced polymer composites: a review on their formation, characteristics, and effects on mechanical performance. *J Compos Mater* 2018; 53(12): 1579–1669.

33. Hernández S, Sket F, Molina-Aldareguí́a JM, et al. Effect of curing cycle on void distribution and interlaminar shear strength in polymer-matrix composites. *Compos Sci Technol* 2011; 71: 1331–1341.

34. Naslain RR. Processing of non-oxide ceramic matrix composites: an overview. *Adv Sci Technology* 2006; 50: 64–74.

35. Vignoles G. Modelling of CVI processes. *Adv Sci Technology* 2006; 50: 97–106.

36. Hemmer J, Dharmalingam AS, Lectez A-S, et al. Compaction behaviour of tow at meso-scale: experimental investigations of morphological evolution at dry, lubricated and saturated states. *IOP Conf Ser Mater Sci Eng* 2018; 406: 012020.

37. Kratz J, Galvez-Hernandez P, Pickard LR, et al. Lab-based in-situ micro-CT observation of gaps in prepreg laminates during consolidation and cure. *Compos A Appl Sci Manuf* 2021; 140: 106180.

38. Khan KA and Umer R. Modeling the viscoelastic compaction response of 3D woven fabrics for liquid composite molding processes. *J Reinf Plast Compos* 2017: 1–17.

39. Latil P, Orgéas L, Geindreau C, et al. Towards the 3D in situ characterization of deformation micro-mechanisms within a compressed bundle of fibres. *Compos Sci Technol* 2011; 71: 480–488.

40. Hemmer J, Burtin C, Comas-Cardona S, et al. Unloading during the infusion process: direct measurement of the dual-scale fibrous microstructure evolution with X-ray computed tomography. *Compos A Appl Sci Manuf* 2018; 115: 147–156.

41. Karaki M, Hallal A, Younes R, et al. A comparative analytical, numerical and experimental analysis of the microscopic permeability of fiber bundles in composite materials. *Int J Compos Mater* 2017; 7(3): 82–102.

42. Larson NM and Zok FW. Insights from in-situ X-ray computed tomography during axial impregnation of unidirectional fiber beds. *Compos A Appl Sci Manuf* 2018; 107134: 124.

43. Centea T and Hubert P. Measuring the impregnation of an out-of-autoclave prepreg by micro-CT. *Compos Sci Technol* 2011; 71: 593–599.

44. Ali MA, Umer R, Khan KA, et al. In-plane virtual permeability characterization of 3D woven fabrics using a hybrid experimental and numerical approach. *Compos Sci Technol* 2019; 173: 99–109.

45. Ali MA, Umer R, Khan KA, et al. XCT-scan assisted flow path analysis and permeability prediction of a 3D woven fabric. *Compos B Eng* 2019; 176: 107320.

46. Vilà J, Sket F, Wilde F, et al. An in situ investigation of microscopic infusion and void transport during vacuum-assisted infiltration by means of X-ray computed tomography. *Compos Sci Technol* 2015; 119: 12–19.

47. Schell JSU, Deleglise M, Binetruy C, et al. Numerical prediction and experimental characterization of meso-scale-

voids in liquid composite moulding. *Compos A Appl Sci Manuf* 2007; 38: 2460–2470.

48. Ali MA, Umer R, Khan KA, et al. Application of X-ray computed tomography for the virtual permeability prediction of fiber reinforcements for liquid composite molding processes: A review. *Compos Sci Technol* 2019; 184: 107828.

49. Sisodia SM, Garcea SC, George AR, et al. High-resolution computed tomography in resin infused woven carbon fibre composites with voids. *Compos Sci Technol* 2016; 131: 12–21.

50. Naouar N, Vidal-Salle E, Schneider J, et al. 3D composite reinforcement meso F.E. analyses based on X-ray computed tomography. *Compos Struct* 2015; 132: 1094–1104.

51. Weglewski W, Bochenek K, Basista M, et al. Comparative assessment of Young's modulus measurements of metal-ceramic composites using mechanical and non-destructive tests and micro-CT based computational modeling. *Comput Mater Sci* 2013; 77: 19–30.

52. Naouar N, Vidal-Sallé E, Schneider J, et al. Meso-scale FE analyses of textile composite reinforcement deformation based on X-ray computed tomography. *Compos Struct* 2014; 116: 165–176.

53. Lee S, Jo E and Ji W. Digital volume correlation technique for characterizing subsurface deformation behavior of a laminated composite. *Compos B Eng* 2020; 194: 108052.

54. Bull DJ, Sinclair I and Spearing SM. Partial volume correction for approximating crack opening displacements in CFRP material obtained from micro-focus X-ray CT scans. *Compos Sci Technol* 2013; 81: 9–16.

55. Brown LP and Long AC. *Composite Reinforcements for Optimum Performance.* Second Edition, 2021, pp. 237–265. Modeling the geometry of textile reinforcements for composites: TexGen

56. Long AC and Brown LP. Modelling the geometry of textile reinforcements for composites: wisetex. *Compos Reinforcements Optimum Perform* 2011: 239–264.

57. Sencu RM, Yang Z, Wang YC, et al. Generation of micro-scale finite element models from synchrotron X-ray CT images for multidirectional carbon fiber reinforced composites. *Compos A Appl Sci Manuf* 2016; 91: 85–95.

58. Czabaj MW, Riccio ML and Whitacre WW. Numerical reconstruction of graphite/epoxy composite microstructure based on sub-micron resolution X-ray computed tomography. *Compos Sci Technol* 2014; 105: 174–182.

59. Aranda-Iglesias D, Giunta G, Peronnet-Paquin A, et al. Multiscale modelling of the mechanical response of 3D multi-axial knitted 3D spacer composites. *Compos Struct* 2021; 257: 113139.

60. Straumit I, Lomov SV and Wevers M. Quantification of the internal structure and automatic generation of voxel models of textile composites from X-ray computed tomography data. *Compos A Appl Sci Manuf* 2015; 69: 150–158.

61. Wu SC, Xiao TQ and Withers PJ. The imaging of failure in structural materials by synchrotron radiation X-ray micro-tomography. *Eng Fract Mech* 2017; 182: 127–156.

62. Haboub A, Bale HA, Nasiatka JR, et al. Tensile testing of materials at high temperatures above 1700°C with in situ synchrotron X-ray micro-tomography. *Rev Sci Instrum* 2014; 85: 083702.

63. Bale HA, Haboub A, MacDowell AA, et al. Real-time quantitative imaging of failure events in materials under load at temperatures above 1,600°C. *Nat Mater* 2012; 12(1): 40–46.

64. Schöberl E, Breite C, Melnikov A, et al. Fibre-direction strain measurement in a composite ply under quasi-static tensile loading using digital volume correlation and in situ synchrotron radiation computed tomography. *Compos A Appl Sci Manuf* 2020; 137: 105935.

65. Li Z, Guo L, Zhang L, et al. In situ experimental investigation on the out-plane damage evolution of 3D woven carbon-fiber reinforced composites. *Compos Sci Technol* 2018; 162: 101–109.

66. Liu B, Hu X, Li Y, et al. Internal three-dimensional strain evolution of the failure process for short carbon fiber composite through in situ synchrotron radiation Xray computed tomography. *Carbon* 2020; 157: 506–514.

67. Hu X, Wang L, Xu F, et al. In situ observations of fractures in short carbon fiber/epoxy composites. *Carbon* 2014; 67: 368–376.

68. Chateau C, Gélébart L, Bornert M, et al. In situ X-ray microtomography characterization of damage in SiCf/SiC minicomposites. *Compos Sci Technol* 2011; 71: 916–924.

69. Hilmas AM, Henson G, Singhal A, et al. In-situ observation of damage in unidirectional CMC laminates under tension. *Ceram Int* 2020; 46: 13502–13510.

70. Zhou W, Qin R, Han K-n, et al. Progressive damage visualization and tensile failure analysis of three-dimensional braided composites by acoustic emission and micro-CT. *Polym Test* 2021; 93: 106881.

71. Wan F, Liu R, Wang Y, et al. In situ observation of compression damage in a 3D needled-punched carbon fiber-silicon carbide ceramic matrix composite. *Compos Struct* 2019; 210: 189–201.

72. Scott AE, Mavrogordato M, Wright P, et al. In situ fiber fracture measurement in carbon-epoxy laminates using high resolution computed tomography. *Compos Sci Technol* 2011; 71: 1471–1477.

73. Zhang P-f, Zhou W, Yin H-f, et al. Progressive damage analysis of three-dimensional braided composites under flexural load by micro-CT and acoustic emission. *Compos Struct* 2019; 226: 111196.

74. Wan F, Liu R, Wang Y, et al. Damage development during flexural loading of a 5-directional braided C/C SiC composite, characterized by X-ray tomography and digital volume correlation. *Ceram Int* 2019; 45: 5601–5612.

75. Sket F, Seltzer R, Molina-Aldareguía JM, et al. Determination of damage micromechanisms and fracture resistance of glass fiber/epoxy cross-ply laminate by means of X-ray computed microtomography. *Compos Sci Technol* 2012; 72: 350–359.

76. Chai Y, Wang Y, Yousaf Z, et al. Damage evolution in braided composite tubes under torsion studied by in-situ X-ray computed tomography. *Compos Sci Technol* 2020; 188: 107976.

77. Yu B, Bradley RS, Soutis C, et al. 2D and 3D imaging of fatigue failure mechanisms of 3D woven composites. *Compos A Appl Sci Manuf* 2015; 77: 37–49.

78. Garcea SC, Mavrogordato MN, Scott AE, et al. Fatigue micromechanism characterization in carbon fiber reinforced polymers using synchrotron radiation computed tomography. *Compos Sci Technol* 2014; 99: 23–30.

79. Garcea SC, Sinclair I and Spearing SM. In situ synchrotron tomographic evaluation of the effect of toughening strategies on fatigue micromechanisms in carbon fiber reinforced polymers. *Compos Sci Technol* 2015; 109: 32–39.

80. Cosmi F and Bernasconi A. Micro-CT investigation on fatigue damage evolution in short fiber reinforced polymers. *Compos Sci Technol* 2016; 79: 70–76.

81. Liu XD, Zhang DT, Qiu HP, et al. On-axis fatigue behaviors and failure characterization of 3D5D braided composites with yarn-reduction using X-ray computed tomography. *Compos Sci Technol* 2021; 203: 108585. DOI: 10.1016/j.compscitech.2020.108585.

82. Yu B, Blanc R, Soutis C, et al. Evolution of damage during the fatigue of 3D woven glass-fibre reinforced composites subjected to tension-tension loading observed by time-lapse X-ray tomography. *Ompos A Appl Sci Manuf* 2016; 82: 279–290.

83. Wagner P, Schwarzhaupt O and May M. In-situ X-ray computed tomography of composites subjected to fatigue loading. *Mater Lett* 2019; 236: 128–130.

84. Qiao Y and Salviato M. Micro-computed tomography analysis of damage in notched composite laminates under multiaxial fatigue. *Compos B Eng* 2020; 187: 107789.

85. Bull DJ, Helfen L, Sinclair I, et al. A comparison of multiscale 3D X-ray tomographic inspection techniques for assessing carbon fibre composite impact damage. *Compos Sci Technol* 2013; 75: 55–61.

86. Barouni AK and Dhakal HN. Damage investigation and assessment due to low-velocity impact on flax/glass hybrid composite plates. *Compos Struct* 2019; 226: 111224.

87. Murugan P, Naresh K, Shankar K, et al. High velocity impact damage investigation of carbon/epoxy/clay nanocomposites using 3D Computed Tomography. *Mater Today Proc* 2018; 5: 16946–16955.

88. Zhou H, Li C, Zhang L, et al. Micro-XCT analysis of damage mechanisms in 3D circular braided composite tubes under transverse impact. *Compos Sci Technol* 2018; 155: 91–99.

89. Fidan S, Sınmazçelik T and Avcu E. Internal damage investigation of the impacted glass/glassþaramid fiber reinforced composites by micro-computerized tomography. *NDT&E Int* 2012; 51: 1–7.

90. Cao W, Zhang J, Sun B, et al. X-ray tomography and numerical study on low-velocity impact damages of three-dimensional angle-interlock woven composites. *Compos Struct* 2019; 230: 111525.

91. Tan KT, Watanabe N and Iwahori Y. X-ray radiography and micro-computed tomography examination of damage characteristics in stitched composites subjected to impact loading. *Compos B Eng* 2011; 42: 874–884.

92. Seltzer R, González C, Muñoz R, et al. X-ray microtomography analysis of the damage micromechanisms in 3D woven composites under low-velocity impact. *Compos A Appl Sci Manuf* 2013; 45: 49–60.

93. Watanabe T, Takeichi Y, Niwa Y, et al. Nanoscale in situ observations of crack initiation and propagation in carbon fiber/epoxy composites using synchrotron radiation X-ray computed tomography. *Compos Sci Technol* 2020; 197: 108244.

94. Borstnar G, Mavrogordato MN, Helfen L, et al. Interlaminar fracture micro-mechanisms in toughened carbon fibre reinforced plastics investigated via synchrotron radiation computed tomography and laminography. *Compos A Appl Sci Manuf* 2015; 71: 176–183.

95. Maillet E, Singhal A, Hilmas A, et al. Combining in-situ synchrotron X-ray microtomography and acoustic emission to characterize damage evolution in ceramic matrix composites. *J Eur Ceram Soc* 2019; 39: 3546–3556.

96. Zeng Q, Sun L, Ge J, et al. Damage characterization and numerical simulation of shear experiment of plain woven glass-fiber reinforced composites based on 3D geometric reconstruction. *Compos Struct* 2020; 233: 111746.

97. Guo L, Huang J, Zhang L, et al. Damage evolution of 3D woven carbon/epoxy composites under tension-tension fatigue loading based on synchrotron radiation computed tomography (SRCT). *Int J Fatigue* 2021; 142: 105913.

98. Zhang D, Liu X, Gu Y, et al. Effects of off-axis angle on shear progressive damage of 3D woven composites with X-ray micro-computed tomography. *Compos A Appl Sci Manuf* 2018; 115: 311–320.

99. Pannier Y, Foti F and Gigliotti M. High temperature fatigue of carbon/polyimide 8-harness satin woven composites. Part I: digital image correlation and micro-computed tomography damage characterization. *Compos Struct* 2020; 244: 112255.

100. Gu Y, Zhang D, Zhang Z, et al. Torsion damage mechanisms analysis of two-dimensional braided composite tubes with digital image correction and X-ray micro-computed tomography. *Compos Struct* 2021; 256: 113020.

101. Wang Y, Burnett TL, Chai Y, et al. X-ray computed tomography study of kink bands in unidirectional composites. *Compos Struct* 2017; 160: 917–924.

102. Garcea SC, Wang Y and Withers PJ. X-ray computed tomography of polymer composites. *Compos Sci Technol* 2018; 156: 305–319.

103. Barbière R, Touchard F, Chocinski-Arnault L, et al. Influence of moisture and drying on fatigue damage mechanisms in a woven hemp/epoxy composite: acoustic emission and micro-CT analysis. *Int J Fatigue* 2020; 136: 105593.

104. Gigliotti M, Pannier Y, Gonzalez RA, et al. X-ray micro-computed-tomography characterization of cracks induced by thermal cycling in non-crimp 3D orthogonal woven composite materials with porosity. *Compos A Appl Sci Manuf* 2018; 112: 100–110.

105. Toubia EA, Sihn S, Pitz J, et al. Thermal response and edgewise compression failure of thermally degraded sandwich composite structures. *Compos Struct* 2021; 256: 113070.

106. Bhreasail ÁN, Lee PD, O'Sullivan C, et al. In-situ observation of cracks in frozen soil using synchrotron tomography. *Permafr Periglac Pro* 2012; 23(2): 170–176.

107. Mei H, Tan Y, Chang P, et al. Simplified approach to study oxidative damage of C/SiC composites induced from notch defects. *Ceram Int* 2019; 45: 22464–22470.

108. Yang H, Lu Z, Bie B, et al. Microstructure and damage evolution of SiCf/PyC/SiC and SiCf/BN/SiC mini-composites: a synchrotron X-ray computed microtomography study. *Ceram Int* 2019; 45: 11395–11402.

109. Thomas J, Bengoa AF, Nori ST, et al. Okuniewski. The application of synchrotron micro-computed tomography to characterize the three-dimensional microstructure in irradiated nuclear fuel. *J Nucl Mater* 2020; 537: 152161.

110. Awaja F, Nguyen M-T, Zhang S, et al. The investigation of inner structural damage of UV and heat degraded polymer composites using X-ray micro CT. *Compos A Appl Sci Manuf* 2011; 42: 408–418.

111. Buffiere JY, Maire E, Adrien J, et al. In situ experiments with X ray tomography: an attractive tool for experimental mechanics. *Exp Mech* 2010; 50: 289–305.

112. Stock SR. X-ray microtomography of materials. *Int Mater Rev* 1999; 44(4): 141–164.

113. Wang Y, Garcea SC and Withers PJ. Computed tomography of composites. *Compr Compos Mat* 2018; 7: 101–108.

114. Kak AC and Slaney M. *Principles of computerized tomographic imaging*. Philadelphia, PA: SIAM, 2001.

115. Stock SR. Recent advances in X-ray microtomography applied to materials. *Int Mater Rev* 2008; 53(3): 129–181.

116. Bronnikov AV. Theory of quantitative phase-contrast computed tomography. *J Opt Soc Am A* 2002; 19(3): 472–480.

117. Centea T, Grunenfelder LK and Nutt SR. A review of out-of-autoclave prepregs-Material properties, process phenomena, and manufacturing considerations. *Compos A Appl Sci Manuf* 2015; 70: 132–154.

118. Böhm R, Stiller J, Behnisch T, et al. A quantitative comparison of the capabilities of in situ computed tomography and conventional computed tomography for damage analysis of composites. *Compos Sci Technol* 2015; 110: 62–68.

119. Garcea SC, Sinclair I and Spearing SM. Fibre failure assessment in carbon fibre reinforced polymers under fatigue loading by synchrotron X-ray computed tomography. *Compos Sci Technol* 2016; 133: 157–164.

120. Teranishi M, Kuwazuru O, Gennai S, et al. Three-dimensional stress and strain around real shape Si particles in cast aluminum alloy under cyclic loading. *Mater Sci Eng A* 2016; 678: 273–285.

121. Kareh KM, Lee PD and Gourlay CM. In situ, time-resolved tomography for validating models of deformation in semi-solid alloys. *IOP Conf Series: Mat Sci Eng* 2012; 33: 012037.

122. Wintiba B, Vasiukov D, Panier S, et al. Automated reconstruction and conformal discretization of 3D woven composite CT scans with local fiber volume fraction control. *Compos Struct* 2020; 248: 112438.

123. Schell JSU, Renggli M, van Lenthe GH, et al. Micro-computed tomography determination of glass fibre reinforced polymer meso-structure. *Compos Sci Technol* 2006; 66: 2016–2022.

124. Liu X, Zhang D, Sun J, et al. Refine reconstruction and verification of meso-scale modeling of three dimensional five-directional braided composites from X-ray computed tomography data. *Compos Struct* 2020; 245: 112347.

125. Sinchuk Y, Pannier Y, Antoranz-Gonzalez R, et al. Analysis of moisture diffusion induced stress in carbon/epoxy 3D textile composite materials with voids by μ-CT based finite element models. *Compos Struct* 2019; 212: 561–570.

126. Sinchuk Y, Pannier Y, Gueguen M, et al. Computed-tomography based modeling and simulation of moisture diffusion and induced swelling in textile composite materials. *Int J Sol Struct* 2018; 154: 88–96.

127. Jing X, Cheng Z, Teng X, et al. Reconstruction of meso-structure and numerical simulations of the mechanical behavior of three-dimensional four-directional braided ceramic matrix composites. *Ceram Int* 2020; 46: 29309–29320.

128. Isart N, El Said B, Ivanov DS, et al. Internal geometric modelling of 3D woven composites: A comparison between different approaches. *Compos Struct* 2015; 132: 1219–1230.

129. Wijaya W, Ali MA, Umer R, et al. An automatic methodology to CT-scans of 2D woven textile fabrics to structured finite element and voxel meshes. *Compos A Appl Sci Manuf* 2019; 125: 105561.

130. Bénézech J and Couégnat G. Variational segmentation of textile composite preforms from X-ray computed tomography. *Compos Struct* 2019; 230: 111496.

131. Tao W, Zhu P, Xu C, et al. Uncertainty quantification of mechanical properties for three-dimensional orthogonal woven composites. Part I: stochastic reinforcement geometry reconstruction. *Compos Struct* 2020; 235: 111763.

132. Rinaldi RG, Blacklock M, Bale H, et al. Generating virtual textile composite specimens using statistical data from micro-computed tomography: 3D tow representations. *J Mech Phys Sol* 2012; 60: 1561–1581.

133. Pan Z, Zhang X, Sun Z, et al. High fidelity simulation of ultrafine PM filtration by multiscale fibrous media characterized by a combination of X-ray CT and FIB-SEM. *J Membr Sci* 2021; 620: 118925.

134. Reh A, Plank B, Kastner J, et al. Porosity maps-interactive exploration and visual analysis of porosity in carbon fiber reinforced polymers. *Euro Vis* 2012; 31(3): 03111.

135. Kastner J, Plank B, Salaberger D, et al. Defect and porosity determination of fibre reinforced polymers by X-ray computed tomography. 2nd International Symposium on NDT Aerosp 2010-We.1. A. 2.

136. Vignoles GL, Germain C, Coindreau O, et al. Fibre-scale modeling of C/C processing by chemical vapor infiltration using Xray CMT images and random walkers. *ECS Transaction* 2009; 25(8): 1275–1284.

137. Yang QD, Schesser D, Niess M, et al. On crack initiation in notched, cross-plied polymer matrix composites. *J Mech Phys Sol* 2015; 78: 314–332.

138. Scott AE, Sinclair I, Spearing SM, et al. Damage accumulation in a carbon/epoxy composite: comparison between a multiscale model and computed tomography experimental results. *Compos A Appl Sci Manuf* 2012; 43: 1514–1522.

139. Perrier A, Touchard F, Chocinski-Arnault L, et al. Quantitative analysis by micro-CT of damage during tensile test in a woven hemp/epoxy composite after water ageing. *Compos A Appl Sci Manuf* 2017; 102: 18–27.

140. Jespersen KM, Zangenberg J, Lowe T, et al. Fatigue damage assessment of uni-directional non-crimp fabric reinforced polyester composite using X-ray computed tomography. *Compos Sci Technol* 2016; 136: 94–103.

141. Withers PJ, Bennett J, Hung Y-C, et al. Crack opening displacements during fatigue crack growth in Ti-SiC fibre metal matrix composites by X-ray tomography. *Mater Sci Eng* 2006; 22(9): 1052–1058.

142. Dau F, Dano M-L and Duplessis-Kergomard Y. Experimental investigations and variability considerations on 3D interlock textile composites used in low velocity soft impact loading. *Compos Struct* 2016; 153: 369–379.

143. Herb V, Martin E and Couégnat G. Damage analysis of thin 3D-woven SiC/SiC composite under low velocity impact loading. *Compos A Appl Sci Manuf* 2012; 43: 247–253.

144. Lu T, Chen X, Wang H, et al. Comparison of low-velocity impact damage in thermoplastic and thermoset composites by non-destructive three-dimensional X-ray microscope. *Polym Test* 2020; 91: 106730.

145. Zhang D, Gu Y, Zhang Z, et al. Effect of off-axis angle on low-velocity impact and compression after impact damage mechanisms of 3D woven composites. *Mater Des* 2020; 192: 108672.

146. Bull DJ, Spearing SM, Sinclair I, et al. Three-dimensional assessment of low velocity impact damage in particle toughened composite laminates using micro-focus X-ray computed tomography and synchrotron radiation laminography. *Compos A Appl Sci Manuf* 2013; 52: 62–69.

147. García-Rodríguez SM, Costa J, Singery V, et al. The effect interleaving has on thin-ply non-crimp fabric laminate impact response: X-ray tomography investigation. *Compos A Appl Sci Manuf* 2018; 107: 409–420.

148. McCombe GP, Rouse J, Trask RS, et al. X-ray damage characterisation in self-healing fibre reinforced polymers. *Compos A Appl Sci Manuf* 2012; 43: 613–620.

149. Hart KR, Chia PXL, Sheridan LE, et al. Mechanisms and characterization of impact damage in 2D and 3D woven fiber-reinforced composites. *Compos A Appl Sci Manuf* 2017; 101: 432–443.